

# Factor Modeling of a High-Dimensional Matrix-Variate and Statistical Learning for Matrix-Valued Sequences

Xu Zhang<sup>1</sup>, Catherine C. Liu<sup>2</sup>, Jianhua Guo<sup>3</sup>, K. C. Yuen<sup>4</sup> and A. H. Welsh<sup>5</sup>

<sup>1</sup>*South China Normal University*, <sup>2</sup>*The Hong Kong Polytechnic University*,

<sup>3</sup>*Beijing Technology and Business University*, <sup>4</sup>*The University of Hong Kong*  
and <sup>5</sup>*The Australian National University*

## Abstract

We propose a new matrix factor model, named RaDFaM, the latent structure of which is strictly derived based on a hierarchical rank decomposition of a matrix. Hierarchy is in the sense that all basis vectors of the column space of each multiplier matrix are assumed the structure of a vector factor model. Compared to the most commonly used matrix factor model that takes the latent structure of a bilinear form, RaDFaM involves additional row-wise and column-wise matrix latent factors. This yields modest dimension reduction and stronger signal intensity from the sight of tensor subspace learning, though poses challenges of new estimation procedure and concomitant inferential theory for a collection of matrix-valued observations. We develop a class of estimation procedure that makes use of the separable covariance structure under RaDFaM and approximate least squares, and derive its superiority in the merit of the peak signal-to-noise ratio. We also establish the asymptotic theory when the matrix-valued observations are uncorrelated or weakly correlated. Numerically, in terms of image/matrix reconstruction, supervised learning, and so forth, we demonstrate the excellent performance of RaDFaM through two matrix-valued sequence datasets of independent 2D images and multinational macroeconomic indices time series, respectively.

*Keywords:* Image reconstruction; Matrix factor model; Peak signal-to-noise ratio; Rank decomposition; Separable covariance structure; Tensor subspace

# 1 Introduction

High-dimensional matrix objects are highly encountered in a broad range of applications, such as the slices of computed tomography (CT) or magnetic resonance imaging (MRI) data in medical imaging, the multinational macroeconomic indices data in economics, to name a few (Zhang, 2017; Gupta and Nagar, 2018; Fan et al., 2020). Out of the noisy observation, to obtain possible low-rank signal that reveals the intrinsic multidimensional structure, the bilinear-form matrix factor model (BiMFaM)

$$\mathbf{X} = \mathbf{S} + \mathbf{e}, \quad \mathbf{S} = \mathbf{R}\mathbf{Z}\mathbf{C}^\top, \quad (1)$$

is widely employed, where up to the noise part  $\mathbf{e}$ , the signal part  $\mathbf{S}$  is a triple product with a low-dimensional latent factor matrix  $\mathbf{Z}$  multiplied by a row loading matrix  $\mathbf{R}$  from the left-hand side and by a column loading matrix  $\mathbf{C}$  from the right-hand side. The estimation and inference under BiMFaM have recently been developed for matrix-valued sequences that are serial correlated or uncorrelated (Wang et al., 2019; Chen and Fan, 2023; Yu et al., 2022).

The bilinear-form latent structure  $\mathbf{R}\mathbf{Z}\mathbf{C}^\top$  is concise in preserving the two-dimensional structural information of the raw high-dimensional matrix object  $\mathbf{X}$ , evidenced by the dimension-folding theory of Li et al. (2010). Nevertheless, the reduced "smaller" latent matrix factor  $\mathbf{Z}$  acts as if the interaction effects of  $\mathbf{X}$  with row-wise and column-wise coefficients  $\mathbf{R}$  and  $\mathbf{C}$ . One may doubt that marginal row-wise and/or column-wise effects are neglected under the bilinear-form latent structure. Take the quarterly multinational, macroeconomic indices collected by the Organisation of Economic Cooperation and Development (OECD) for instance. Such samples can be treated as matrix-variate observations (one for each quarter) with rows, columns, and each entry representing different countries, macroeconomic indices, and the value of the index of the corresponding country, respectively.

Figure 1 (a), (b), and (c) show correlation heatmaps of the row-wise (country), column-wise (index), and the interaction between rows and columns, respectively. Figure 1 (c) displays the existence of sign-varying correlation across different rows and columns, as can be anticipated from BiMFaM. Nevertheless, Figure 1 (a) reflects the existence of significant positive correlations among countries (rows) because of their geographical, historical, economic, and political relationships; Figure 1 (b) reveals the existence of correlations among indices (columns), such as the CPI group and the international trade group. Consequently, neglecting the pure row or column information as BiMFaM does, may impair unsupervised

learning. This will be illustrated in our numerical results later.

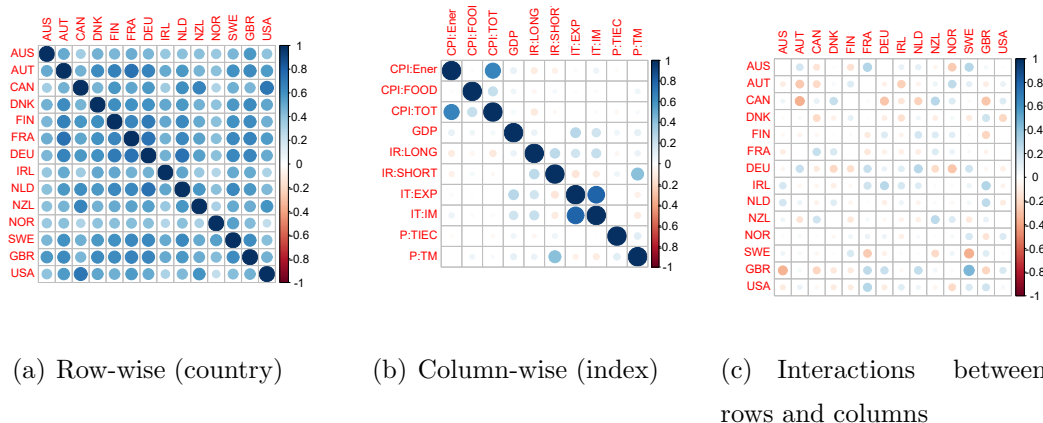


Figure 1: Observed correlations in the multinational, macroeconomic indices data.

The above analysis motivates us to present a factor model with new latent structure from the insight of the general rank decomposition of a matrix object, yielding a low-rank approximation with three summands involving global, row-wise, and column-wise latent factors respectively. We attempt to use tensor subspace concepts to explain that, although incorporating two mode-wise additional latent factors slows down the theoretical convergence rate of the estimated loading matrices, the reconstruction performance behaves better than using just the bilinear-form signal without an extra computational burden. In addition, the complicated structure makes the estimation procedure challenging. The spectral method (or the method of principal components) that is suitable for BiMFaM is not directly applicable to estimate the common components or signal under the newly proposed matrix factor model. From the distributional point of view, the proposed model can be regarded as the explicit model form of a matrix-variate distribution with separable covariance structure (Dawid, 1981; Hoff, 2011; Gupta and Nagar, 2018). This observation inspires our separable PCA estimation for the loading matrix parameters, followed by approximate least square estimation for the factor matrices and the common components. Last but not least, our estimators tackle matrix-variate observations effectively regardless of the uncorrelation or correlation of the sequence.

The remainder of this article is organized as follows. Section 2 derives our new latent structure for matrix objects and compares it with BiMFaM. Section 3 develops estimators for the components in the low-rank approximation based on matrix-variate observations and reconstruction error theory. Section 4 establishes the asymptotic theory and Section 5 presents simulation studies that evaluate the finite sample performance of the method.

Section 6 analyzes the CT image data collected early in the COVID-19 pandemic, and the multinational macroeconomic indices data for the purpose of supervised learning, image/matrix reconstruction, and so forth. Section 7 concludes the paper with some further research topics. All the technical proofs are given in the online supplement.

## 2 Rank-Decomposition-Based Matrix Factor Model

### 2.1 Modeling Low-Rank Approximation

Recall that a matrix  $\mathbf{X} \in \mathbb{R}^{p_1 \times p_2}$  of rank- $l$  has the general rank decomposition or factorization in the sense that  $\mathbf{X} = \mathbf{U}\mathbf{V}^\top$ , where  $\mathbf{U} = (\mathbf{U}_1, \dots, \mathbf{U}_l) \in \mathbb{R}^{p_1 \times l}$  and  $\mathbf{V} = (\mathbf{V}_1, \dots, \mathbf{V}_l) \in \mathbb{R}^{p_2 \times l}$  are *full column rank matrices*. Let  $\text{span}(\mathbf{M})$  be the *column space* spanned by the columns of the placeholder matrix  $\mathbf{M}$ . Then  $\{\mathbf{U}_i\}_{i=1}^l$  and  $\{\mathbf{V}_i\}_{i=1}^l$  are *basis* of  $\text{span}(\mathbf{U})$  and  $\text{span}(\mathbf{V})$ , respectively.

For a high-dimensional matrix-variate  $\mathbf{X}$ , where  $p_1$  and  $p_2$  can tend to infinity, by all basis vectors endowed with the vector factor model structure, we postulate the following rank-decomposition-based matrix factor model (RaDFaM),

$$\begin{cases} \mathbf{X} = \mathbf{U}\mathbf{V}^\top = \sum_{i=1}^l \mathbf{U}_i \mathbf{V}_i^\top, & (\text{rank-}l \text{ decomposition}) \\ \mathbf{U}_i = \mathbf{R}\mathbf{A}_i + \boldsymbol{\xi}_i, \quad \mathbf{V}_i = \mathbf{C}\mathbf{B}_i + \boldsymbol{\eta}_i, & (\text{vector factor models}) \end{cases} \quad (2)$$

where  $\mathbf{R} \in \mathbb{R}^{p_1 \times k_1}$  ( $k_1 \ll p_1$ ) and  $\mathbf{C} \in \mathbb{R}^{p_2 \times k_2}$  ( $k_2 \ll p_2$ ) are the matrices of factor loadings,  $\mathbf{A}_i \in \mathbb{R}^{k_1}$  and  $\mathbf{B}_i \in \mathbb{R}^{k_2}$  are the vectors of common factors, and  $\boldsymbol{\xi}_i \in \mathbb{R}^{p_1}$  and  $\boldsymbol{\eta}_i \in \mathbb{R}^{p_2}$  are the vectors of idiosyncratic errors.

To brief the hierarchical structure in expression (2), we adopt matrix notation to denote  $\mathbf{A} = (\mathbf{A}_1, \dots, \mathbf{A}_l)^\top \in \mathbb{R}^{l \times k_1}$ ,  $\mathbf{B} = (\mathbf{B}_1, \dots, \mathbf{B}_l)^\top \in \mathbb{R}^{l \times k_2}$ ,  $\boldsymbol{\xi} = (\boldsymbol{\xi}_1, \dots, \boldsymbol{\xi}_l) \in \mathbb{R}^{p_1 \times l}$ , and  $\boldsymbol{\eta} = (\boldsymbol{\eta}_1, \dots, \boldsymbol{\eta}_l) \in \mathbb{R}^{p_2 \times l}$ . Let  $\mathbf{Z} = \mathbf{A}^\top \mathbf{B} \in \mathbb{R}^{k_1 \times k_2}$ ,  $\mathbf{E} = \boldsymbol{\eta} \mathbf{A} \in \mathbb{R}^{p_2 \times k_1}$ ,  $\mathbf{F} = \boldsymbol{\xi} \mathbf{B} \in \mathbb{R}^{p_1 \times k_2}$ , and  $\mathbf{e} = \boldsymbol{\xi} \boldsymbol{\eta}^\top \in \mathbb{R}^{p_1 \times p_2}$ . Then the equivalence of model (2) can be expressed as

$$\mathbf{X} = \mathbf{S} + \mathbf{e}, \quad \mathbf{S} = \mathbf{R}\mathbf{Z}\mathbf{C}^\top + \mathbf{R}\mathbf{E}^\top + \mathbf{F}\mathbf{C}^\top, \quad (3)$$

where  $\mathbf{S} \in \mathbb{R}^{p_1 \times p_2}$  represents the unobserved low-rank signal, and  $\mathbf{e}$  is the noise matrix. We may call  $\mathbf{Z}$ ,  $\mathbf{E}$ , and  $\mathbf{F}$  the *global*, *column-wise*, and *row-wise* latent factor matrices, respectively; and  $\mathbf{R}$  and  $\mathbf{C}$  are the *row-wise* and *column-wise* loading matrices, respectively.

## 2.2 Tensor Subspace Learning: RaDFaM v.s. BiMFaM

From the perspective of tensor subspace learning (He et al., 2005; Lu et al., 2013), the low-dimensional tensor subspace of the low-rank signal matrix  $\mathbf{S}$  of RaDFaM (3) can be written as

$$\mathcal{S}_{RaD} = \left\{ \sum_{i_1=1}^{k_1} \sum_{i_2=1}^{k_2} \mathbf{Z}_{i_1 i_2} (\mathbf{R}_{i_1} \circ \mathbf{C}_{i_2}) + \sum_{i_1=1}^{k_1} \sum_{i_2=1}^{p_2} \mathbf{E}_{i_2 i_1} (\mathbf{R}_{i_1} \circ \mathbf{I}_{p_2, i_2}) + \sum_{i_1=1}^{p_1} \sum_{i_2=1}^{k_2} \mathbf{F}_{i_1 i_2} (\mathbf{I}_{p_1, i_1} \circ \mathbf{C}_{i_2}) \right. \\ \left. | \mathbf{Z} = (\mathbf{Z}_{i_1 i_2}) \in \mathbb{R}^{k_1 \times k_2}, \mathbf{E} = (\mathbf{E}_{i_2 i_1}) \in \mathbb{R}^{p_2 \times k_1}, \mathbf{F} = (\mathbf{F}_{i_1 i_2}) \in \mathbb{R}^{p_1 \times k_2} \right\}, \quad (4)$$

where  $\circ$  is the outer product operation,  $\mathbf{R}_{i_1}$  and  $\mathbf{C}_{i_2}$  are the  $i_1$ th and the  $i_2$ th columns of  $\mathbf{R}$  and  $\mathbf{C}$ , and  $\mathbf{I}_{p_1, i_1}$  and  $\mathbf{I}_{p_2, i_2}$  are the  $i_1$ th and the  $i_2$ th columns of the  $p_1$ -dim and  $p_2$ -dim identity matrices.

To demonstrate the dimension of  $\mathcal{S}_{RaD}$ , we use the tensor product (Greub, 1978, Chapter 1). A tensor product of two vector spaces  $V$  and  $W$  is a vector space denoted  $V \otimes_T W$  (pronounced  $V$  tensor  $W$ ), where  $\otimes_T$  is a bilinear map  $\otimes_T : V \times_T W \rightarrow V \otimes_T W$ ,  $(v, w) \mapsto v \otimes_T w$  satisfying the universal property, i.e., for any bilinear map  $b : V \times W \rightarrow U$  there is a unique linear map  $\bar{b} : V \otimes_T W \rightarrow U$  such that  $\bar{b}(v \otimes_T w) = b(v, w)$ . In addition, If  $\{v_i\}$  and  $\{w_j\}$  are bases of  $V$  and  $W$ , respectively, then  $\{v_i \otimes_T w_j\}$  is a basis of  $V \otimes_T W$ .

Let  $\text{vec}(\cdot)$  denote the vectorization operation and  $[n] = \{1, \dots, n\}$  with  $n$  as the placeholder. Taking the bilinear map  $\otimes_T$  as the Kronecker product  $\otimes$ , we have  $\text{vec}(\mathbf{R}_{i_1} \circ \mathbf{C}_{i_2}) = \mathbf{C}_{i_2} \otimes \mathbf{R}_{i_1}$ ,  $\text{vec}(\mathbf{R}_{i_1} \circ \mathbf{I}_{p_2, i_2}) = \mathbf{I}_{p_2, i_2} \otimes \mathbf{R}_{i_1}$ , and  $\text{vec}(\mathbf{I}_{p_1, i_1} \circ \mathbf{C}_{i_2}) = \mathbf{C}_{i_2} \otimes \mathbf{I}_{p_1, i_1}$ . Then  $\{\mathbf{C}_{i_2} \otimes \mathbf{R}_{i_1} : i_1 \in [k_1], i_2 \in [k_2]\}$ ,  $\{\mathbf{I}_{p_2, i_2} \otimes \mathbf{R}_{i_1} : i_1 \in [k_1], i_2 \in [p_2]\}$  and  $\{\mathbf{C}_{i_2} \otimes \mathbf{I}_{p_1, i_1} : i_1 \in [p_1], i_2 \in [k_2]\}$  are bases of the tensor products  $\text{span}(\mathbf{C}) \otimes \text{span}(\mathbf{R})$ ,  $\mathbb{R}^{p_2} \otimes \text{span}(\mathbf{R})$  and  $\text{span}(\mathbf{C}) \otimes \mathbb{R}^{p_1}$ , respectively. We can see that  $\text{span}(\mathbf{C}) \otimes \text{span}(\mathbf{R})$  is contained in  $\mathbb{R}^{p_2} \otimes \text{span}(\mathbf{R})$  or  $\text{span}(\mathbf{C}) \otimes \mathbb{R}^{p_1}$ . As a result, the tensor subspace  $\mathcal{S}_{RaD}$  maps to the vectorization subspace

$$\tilde{\mathcal{S}}_{RaD} = \left\{ \sum_{i_1=1}^{k_1} \sum_{i_2=1}^{k_2} \mathbf{Z}_{i_1 i_2} (\mathbf{C}_{i_2} \otimes \mathbf{R}_{i_1}) + \sum_{i_1=1}^{k_1} \sum_{i_2=1}^{p_2} \mathbf{E}_{i_2 i_1} (\mathbf{I}_{p_2, i_2} \otimes \mathbf{R}_{i_1}) + \sum_{i_1=1}^{p_1} \sum_{i_2=1}^{k_2} \mathbf{F}_{i_1 i_2} (\mathbf{C}_{i_2} \otimes \mathbf{I}_{p_1, i_1}) \right. \\ \left. | \mathbf{Z} = (\mathbf{Z}_{i_1 i_2}) \in \mathbb{R}^{k_1 \times k_2}, \mathbf{E} = (\mathbf{E}_{i_2 i_1}) \in \mathbb{R}^{p_2 \times k_1}, \mathbf{F} = (\mathbf{F}_{i_1 i_2}) \in \mathbb{R}^{p_1 \times k_2} \right\}.$$

Therefore, the dimension of  $\tilde{\mathcal{S}}_{RaD}$  or  $\mathcal{S}_{RaD}$  is

$$\dim(\mathcal{S}_{RaD}) = \dim(\tilde{\mathcal{S}}_{RaD}) = p_1 k_2 + k_1 p_2 - \dim\{\text{span}(\mathbf{I}_{p_2} \otimes \mathbf{R}) \cap \text{span}(\mathbf{C} \otimes \mathbf{I}_{p_1})\} \ll p_1 p_2.$$

The corresponding low-dimensional tensor subspace and vectorization subspace of the low-rank signal matrix of BiMFaM are

$$\mathcal{S}_{BiM} = \left\{ \sum_{i_1=1}^{k_1} \sum_{i_2=1}^{k_2} \mathbf{Z}_{i_1 i_2} (\mathbf{R}_{i_1} \circ \mathbf{C}_{i_2}) | \mathbf{Z} = (\mathbf{Z}_{i_1 i_2}) \in \mathbb{R}^{k_1 \times k_2} \right\}, \quad (5) \\ \tilde{\mathcal{S}}_{BiM} = \left\{ \sum_{i_1=1}^{k_1} \sum_{i_2=1}^{k_2} \mathbf{Z}_{i_1 i_2} (\mathbf{C}_{i_2} \otimes \mathbf{R}_{i_1}) | \mathbf{Z} = (\mathbf{Z}_{i_1 i_2}) \in \mathbb{R}^{k_1 \times k_2} \right\},$$

respectively, with  $\dim(\mathcal{S}_{BiM}) = \dim(\tilde{\mathcal{S}}_{BiM}) = k_1 k_2$ .

From the comparison between  $\mathcal{S}_{BiM}$  and  $\mathcal{S}_{RaD}$ , we can see that RaDFaM takes the strategy of modest dimension reduction in the sense that  $\dim(\mathcal{S}_{RaD})$  is larger than  $\dim(\mathcal{S}_{BiM})$ . This decent “larger” fact obviously strengthens the signal intensity, and meanwhile the identical unknown basis parameters  $\mathbf{R}$  and  $\mathbf{C}$  incur no extra computation burden. Nevertheless, due to the additional column-wise and row-wise latent factor matrices  $\mathbf{E}$  and  $\mathbf{F}$ , the latent structure of RaDFaM is more complex. Consequently, for a collection of matrix-valued dataset, the existing estimation of latent factor matrices under BiMFaM is infeasible under RaDFaM and it calls for new estimation for  $\mathbf{Z}$ ,  $\mathbf{E}$  and  $\mathbf{F}$ .

### 2.3 Separable Covariance Structure of RaDFaM

In this subsection, we will derive that a matrix-variate  $\mathbf{X}$  rank  $l$  under RaDFaM possesses the property of separable covariance structure. A matrix-variate is said to have separable covariance structure if its covariance model is parameterized in terms of both row-wise and column-wise covariance matrices; mathematically the covariance matrix of the vectorized matrix-variate  $\text{vec}(\mathbf{X})$  is expressible in the form of the Kronecker products of the column-wise covariance matrix  $\Sigma_2$  and the row-wise covariance matrix  $\Sigma_1$  (Hoff, 2011; Fosdick and Hoff, 2014).

To this end, we need some common assumptions on the relation among the components that appear in model (2) or its equivalence model (3). The factor matrix  $\mathbf{A}$  and the noise matrix  $\xi$  are uncorrelated, and  $\mathbf{A}$  and  $\xi$  are uncorrelated across rows and columns respectively; and so are the pair  $(\mathbf{B}, \eta)$ . Let  $\Psi_A$  be the row-wise covariance matrix of  $\mathbf{A}$  and  $\Psi_\xi$  be the column-wise covariance matrix of  $\xi$ ; and so are the pair  $(\Psi_B, \Psi_\eta)$ . In addition,  $\mathbf{A}$ ,  $\mathbf{B}$ ,  $\xi$ , and  $\eta$  in model (2) are zero mean and mutually uncorrelated, which imply the zero mean and mutually uncorrelation of  $\mathbf{Z}$ ,  $\mathbf{E}$ ,  $\mathbf{F}$ , and  $\mathbf{e}$  in model (3). These are quite general assumptions under the factor model setting in the last two decades and are omitted in the below proposition.

**Proposition 1** (*Separable covariance structure*) *For matrix-variate  $\mathbf{X}$ , under the latent structure given by RaDFaM, we have*

$$\text{cov}\{\text{vec}(\mathbf{X})\} = l(\Sigma_2 \otimes \Sigma_1),$$

where  $\Sigma_1 = \mathbf{R}\Psi_A\mathbf{R}^\top + \Psi_\xi \in \mathbb{R}^{p_1 \times p_1}$  and  $\Sigma_2 = \mathbf{C}\Psi_B\mathbf{C}^\top + \Psi_\eta \in \mathbb{R}^{p_2 \times p_2}$ .

*Proof:* By vectorizing model (3) and incorporating the representation from model (2), we have

$$\begin{aligned}
\text{vec}(\mathbf{X}) &= (\mathbf{C} \otimes \mathbf{R})\text{vec}(\mathbf{Z}) + (\mathbf{I}_{p_2} \otimes \mathbf{R})\text{vec}(\mathbf{E}^\top) + (\mathbf{C} \otimes \mathbf{I}_{p_1})\text{vec}(\mathbf{F}) + \text{vec}(\mathbf{e}) \\
&= (\mathbf{C} \otimes \mathbf{R}) \sum_{m=1}^l (\mathbf{B}_{m\cdot} \otimes \mathbf{A}_{m\cdot}) + (\mathbf{I}_{p_2} \otimes \mathbf{R}) \sum_{m=1}^l (\boldsymbol{\eta}_m \otimes \mathbf{A}_{m\cdot}) \\
&\quad + (\mathbf{C} \otimes \mathbf{I}_{p_1}) \sum_{m=1}^l (\mathbf{B}_{m\cdot} \otimes \boldsymbol{\xi}_m) + \sum_{m=1}^l (\boldsymbol{\eta}_m \otimes \boldsymbol{\xi}_m).
\end{aligned}$$

Then some algebra shows that

$$\begin{aligned}
&\mathbb{E}\{\text{vec}(\mathbf{X})\text{vec}^\top(\mathbf{X})\} \\
&= l\mathbf{C}\boldsymbol{\Psi}_B\mathbf{C}^\top \otimes \mathbf{R}\boldsymbol{\Psi}_A\mathbf{R}^\top + l\boldsymbol{\Psi}_\eta \otimes \mathbf{R}\boldsymbol{\Psi}_A\mathbf{R}^\top + l\mathbf{C}\boldsymbol{\Psi}_B\mathbf{C}^\top \otimes \boldsymbol{\Psi}_\xi + l\boldsymbol{\Psi}_\eta \otimes \boldsymbol{\Psi}_\xi \\
&= l(\mathbf{C}\boldsymbol{\Psi}_B\mathbf{C}^\top + \boldsymbol{\Psi}_\eta) \otimes (\mathbf{R}\boldsymbol{\Psi}_A\mathbf{R}^\top + \boldsymbol{\Psi}_\xi). \quad \square
\end{aligned}$$

Proposition 1 characterizes dependence along row-wise and column-wise of a matrix variate under RaDFaM. Taking the covariance matrix among different rows of  $\mathbf{X}$  as an example, it is readily to obtain that the covariance matrix between the  $i_1$ th and  $i_2$ th rows is

$$\mathbb{E}(\mathbf{X}_{i_1\cdot}\mathbf{X}_{i_2\cdot}^\top) = l\boldsymbol{\Sigma}_{1,i_1i_2}\boldsymbol{\Sigma}_2, \quad i_1, i_2 \in [p_1], \quad (6)$$

where  $\boldsymbol{\Sigma}_{1,i_1i_2}$  is the  $(i_1, i_2)$ th element of  $\boldsymbol{\Sigma}_1$  that controls the correlation between the  $i_1$ th and  $i_2$ th rows, and  $\boldsymbol{\Sigma}_2$  represents the general row-wise correlation structure. Analogous to the above analysis, the elements of  $\boldsymbol{\Sigma}_2$  controls the correlation of different columns, and  $\boldsymbol{\Sigma}_1$  represents the general column-wise correlation structure.

Compared to BiMFaM, such separable covariance structure is unique for RaDFaM owing to the additional row-wise and column-wise latent factor matrices  $\mathbf{F}$  and  $\mathbf{E}$ . It actually inspires the derivation of the estimation of loading matrices in Subsection 3.1.

**Remark 1.** *Contribution of three matrix latent factors.* The fact that RadFaM has separable covariance structure will foster our understanding of the three matrix latent factors. The element-wise covariance of  $\mathbf{X}$  is readily derived based on equation (6) together with the expressions of  $\boldsymbol{\Sigma}_1$  and  $\boldsymbol{\Sigma}_2$ ,

$$\mathbb{E}(\mathbf{X}_{i_1j_1}\mathbf{X}_{i_2j_2}) = \mathbf{R}_{i_1\cdot}^\top \mathbb{E}(\mathbf{Z}\mathbf{C}_{j_1\cdot}^\top \mathbf{C}_{j_2\cdot}^\top \mathbf{Z}^\top) \mathbf{R}_{i_2\cdot} + \mathbf{R}_{i_1\cdot}^\top \mathbb{E}(\mathbf{E}_{j_1\cdot} \mathbf{E}_{j_2\cdot}^\top) \mathbf{R}_{i_2\cdot} + \mathbf{C}_{j_1\cdot}^\top \mathbb{E}(\mathbf{F}_{i_1\cdot} \mathbf{F}_{i_2\cdot}^\top) \mathbf{C}_{j_2\cdot} + \mathbb{E}(\mathbf{e}_{i_1j_1} \mathbf{e}_{i_2j_2}).$$

Under the special case of diagonality of  $\boldsymbol{\Psi}_\xi$  and  $\boldsymbol{\Psi}_\eta$ , or equivalently the uncorrelation of the rows of  $\mathbf{F}$ ,  $\mathbf{E}$ , and elements of  $\mathbf{e}$ , the first summand related to  $\mathbf{Z}$  is nonzero for any quadruple  $(i_1, j_1, i_2, j_2)$ , the second summand related to  $\mathbf{E}$  is nonzero only for two entries in the same

column (i.e.,  $j_1 = j_2$ ), and the third summand related to  $\mathbf{F}$  is nonzero only for two entries in the same row (i.e.,  $i_1 = i_2$ ), respectively. This fact implies that the global latent factor  $\mathbf{Z}$  combines the row-wise, column-wise, and the across modes correlation of the matrix variate, the row-wise latent factor  $\mathbf{F}$  reflects the pure row-wise correlation of the matrix variate, and the column-wise latent factor  $\mathbf{E}$  reflects the pure column-wise correlation of the matrix variate, respectively.

### 3 Estimation under RaDFaM for Matrix-Valued Observations

Let  $\mathbf{X}_t \in \mathbb{R}^{p_1 \times p_2}$ ,  $t \in [T]$ , be a sequence of high-dimensional matrix-valued observations that might be weakly correlated or uncorrelated, where the mode-wise dimensions  $p_1$  and  $p_2$ , and the number of observations  $T$  can all tend to infinity. Then RaDFaM with observations  $\mathbf{X}_t$  yields

$$\mathbf{X}_t = \mathbf{S}_t + \mathbf{e}_t, \quad \mathbf{S}_t = \mathbf{R}\mathbf{Z}_t\mathbf{C}^\top + \mathbf{R}\mathbf{E}_t^\top + \mathbf{F}_t\mathbf{C}^\top. \quad (7)$$

In this section, under model+data in (7), we propose a set of estimation for components in the signal part, and show that RaDFaM has stronger peak signal-to-noise ratio compared to BiMFaM.

#### 3.1 Separable PCA Estimators for Loading Matrices

It is known that estimates of loading matrices  $\mathbf{R}$  and  $\mathbf{C}$  are only unique up to rotation (Wang et al., 2019; Chen and Fan, 2023). Thus we restrict the loading matrices by  $p_1^{-1}\mathbf{R}^\top\mathbf{R} = \mathbf{I}_{k_1}$  and  $p_2^{-1}\mathbf{C}^\top\mathbf{C} = \mathbf{I}_{k_2}$  known as the strong factor assumption in the literature of factor models (Stock and Watson, 2002; Lam and Yao, 2011). In Assumption 3 of Section 4, we use the strict limit form of the strong factor assumption.

The spectral or the principal components methods that are most commonly used for estimation of loading matrices are based on eigen-decomposition or singular value decomposition of some moment-variant statistics (Chen and Fan, 2023, Remark 2). One of the rationale behind these methods is that under the strong factor assumption, the eigenspaces spanned by the top eigenvectors of population moment matrices are consistent estimators for column spaces of loading matrices (Davis and Kahan, 1970).



Nonetheless, under model (7) for matrix-variate observations, spectral methods may be troublesome. Take the row-wise population variance-covariance matrix for instance

$$\mathbb{E}(\mathbf{X}_t \mathbf{X}_t^\top) = p_2 \mathbf{R} \mathbb{E}(\mathbf{Z}_t \mathbf{Z}_t^\top) \mathbf{R}^\top + \{\mathbf{R} \mathbb{E}(\mathbf{E}_t^\top \mathbf{E}_t) \mathbf{R}^\top + p_2 \mathbb{E}(\mathbf{F}_t \mathbf{F}_t^\top)\} + \mathbb{E}(\mathbf{e}_t \mathbf{e}_t^\top). \quad (8)$$

Compared to BiMFaM, the two terms in the brace of the right-hand side are not negligible due to the column-wise and row-wise latent factor matrices  $\mathbf{E}_t$  and  $\mathbf{F}_t$ . Fortunately, according to Proposition 1, we have the following proposition.

**Proposition 2** (*Row-wise population variance-covariance matrix*) Under RaDFaM, based on the separable covariance structure in Proposition 1, we have

$$\mathbb{E}(\mathbf{X}_t \mathbf{X}_t^\top) = \{\text{ltr}(\boldsymbol{\Sigma}_2)\} \boldsymbol{\Sigma}_1.$$

*Proof:* Some simple algebra gives

$$\mathbb{E}(\mathbf{X}_t \mathbf{X}_t^\top) = \sum_{j=1}^{p_2} \mathbb{E}(\mathbf{X}_{t,j} \mathbf{X}_{t,j}^\top) = (l \sum_{j=1}^{p_2} \boldsymbol{\Sigma}_{2,jj}) \boldsymbol{\Sigma}_1 = \{\text{ltr}(\boldsymbol{\Sigma}_2)\} \boldsymbol{\Sigma}_1. \quad \square$$

Proposition 2 demonstrates the equivalence of top eigenspaces of  $\mathbb{E}(\mathbf{X}_t \mathbf{X}_t^\top)$  and  $\boldsymbol{\Sigma}_1$ . Denote  $\text{eig}(\mathbf{M}, r)$  as a matrix with columns given by the top  $r$  eigenvectors of the placeholder matrix  $\mathbf{M}$ . Then we have

$$\text{span}[\text{eig}\{\mathbb{E}(\mathbf{X}_t \mathbf{X}_t^\top), k_1\}] = \text{span}\{\text{eig}(\boldsymbol{\Sigma}_1, k_1)\}. \quad (9)$$

Recall that  $\boldsymbol{\Sigma}_1 = \mathbf{R} \boldsymbol{\Psi}_A \mathbf{R}^\top + \boldsymbol{\Psi}_\xi$ . Using the pervasiveness assumption and applying the Davis-Kahan Theorem (Fan et al., 2020; Davis and Kahan, 1970), one can show the approximate equivalence between the top eigenspace of  $\boldsymbol{\Sigma}_1$  and the column space of  $\mathbf{R}$

$$\frac{1}{p_1} \|\text{eig}(\boldsymbol{\Sigma}_1, k_1) \text{eig}^\top(\boldsymbol{\Sigma}_1, k_1) - \mathbf{R} \mathbf{R}^\top\|_F = o(1). \quad (10)$$

Hence, based on (9) and (10), we have the approximate equivalence of top eigenspace of  $\mathbb{E}(\mathbf{X}_t \mathbf{X}_t^\top)$  and the column space of  $\mathbf{R}$

$$\text{span}[\text{eig}\{\mathbb{E}(\mathbf{X}_t \mathbf{X}_t^\top), k_1\}] \approx \text{span}(\mathbf{R}). \quad (11)$$

It is safe now to derive the spectral estimator of  $\mathbf{R}$  as

$$\hat{\mathbf{R}} = \sqrt{p_1} \text{eig}(\widehat{\mathbf{M}}_1, k_1) \quad \text{with} \quad \widehat{\mathbf{M}}_1 = \frac{1}{T p_1 p_2} \sum_{t=1}^T \mathbf{X}_t \mathbf{X}_t^\top.$$

Analogous to the above analysis, the spectral estimator of  $\mathbf{C}$  is

$$\widehat{\mathbf{C}} = \sqrt{p_2} \text{eig}(\widehat{\mathbf{M}}_2, k_2) \quad \text{with} \quad \widehat{\mathbf{M}}_2 = \frac{1}{Tp_1p_2} \sum_{t=1}^T \mathbf{X}_t^\top \mathbf{X}_t.$$

Note that equation (11) and its corresponding column-wise counterpart guarantee the feasibility of such spectral methods for estimating loading matrices. The separable covariance structure assures equation (11) under RaDFaM, whilst equation (11) is obvious under BiM-FaM. Hence, estimators  $\widehat{\mathbf{R}}$  and  $\widehat{\mathbf{C}}$  are identical under BiMFaM and RaDFaM. This coincides with the fact that the basis parameters are the same in tensor subspaces  $\mathcal{S}_{RaD}$  (4) and  $\mathcal{S}_{BiM}$  (5).

**Remark 2.** *Factor scores and signal parts.* Under BiMFaM, an estimator of  $\mathbf{Z}_t$  is obtained straightforwardly by multiplying the left and the right hand sides of  $\mathbf{X}_t$  by  $\widehat{\mathbf{R}}$  and  $\widehat{\mathbf{C}}$ , respectively. Similarly, for  $\mathbf{S}_t$ , we obtain

$$\widetilde{\mathbf{Z}}_t = \frac{\widehat{\mathbf{R}}^\top \mathbf{X}_t \widehat{\mathbf{C}}}{p_1 p_2} \quad \text{and} \quad \widetilde{\mathbf{S}}_t = \frac{\widehat{\mathbf{R}} \widehat{\mathbf{R}}^\top \mathbf{X}_t \widehat{\mathbf{C}} \widehat{\mathbf{C}}^\top}{p_1 p_2}. \quad (12)$$

However, this is not applicable under RaDFaM because of the presence of the two mode-wise latent factor matrices  $\mathbf{E}_t$  and  $\mathbf{F}_t$ . Under RaDFaM, direct bilateral multiplication on  $\mathbf{X}_t$  yields two additional terms  $\mathbf{E}_t^\top \widehat{\mathbf{C}}$  and  $\widehat{\mathbf{R}}^\top \mathbf{F}_t$  that also need to be estimated.

### 3.2 Least Square Estimators for Factor Matrices

To obtain estimators  $\widehat{\mathbf{Z}}_t$ ,  $\widehat{\mathbf{E}}_t$ , and  $\widehat{\mathbf{F}}_t$  of the factor matrices in RaDFaM, we solve the (error of matrix reconstruction) minimization problem

$$\min_{\substack{p_1^{-1} \mathbf{R}^\top \mathbf{R} = \mathbf{I}_{k_1}, p_2^{-1} \mathbf{C}^\top \mathbf{C} = \mathbf{I}_{k_2} \\ \{\mathbf{Z}_t\}_{t=1}^T, \{\mathbf{E}_t\}_{t=1}^T, \{\mathbf{F}_t\}_{t=1}^T}} \frac{1}{Tp_1p_2} \sum_{t=1}^T \|\mathbf{X}_t - \mathbf{R} \mathbf{Z}_t \mathbf{C}^\top - \mathbf{R} \mathbf{E}_t^\top - \mathbf{F}_t \mathbf{C}^\top\|_F^2,$$

where  $\|\cdot\|_F$  is the Frobenius norm. We use the equations  $p_1^{-1} \mathbf{R}^\top \mathbf{R} = \mathbf{I}_{k_1}$  and  $p_2^{-1} \mathbf{C}^\top \mathbf{C} = \mathbf{I}_{k_2}$  directly to simplify the derivation in this subsection. Using the fact that  $\|\mathbf{A}\|_F^2 = \text{tr}(\mathbf{A} \mathbf{A}^\top)$ , we expand the objective function, and then take partial derivatives with respect to  $\mathbf{Z}_t$ ,  $\mathbf{F}_t$ , and  $\mathbf{E}_t$  to obtain the normal equations. After some algebra, we obtain the system of equations

$$\begin{cases} \mathbf{Z}_t = \frac{\mathbf{R}^\top \mathbf{X}_t \mathbf{C}}{p_1 p_2} - \frac{\mathbf{E}_t^\top \mathbf{C}}{p_2} - \frac{\mathbf{R}^\top \mathbf{F}_t}{p_1}, \\ (\mathbf{I}_{p_1} - \frac{\mathbf{R} \mathbf{R}^\top}{p_1}) (\mathbf{F}_t - \frac{\mathbf{X}_t \mathbf{C}}{p_2}) = \mathbf{0}_{p_1 \times k_2}, \\ (\mathbf{I}_{p_2} - \frac{\mathbf{C} \mathbf{C}^\top}{p_2}) (\mathbf{E}_t - \frac{\mathbf{X}_t^\top \mathbf{R}}{p_1}) = \mathbf{0}_{p_2 \times k_1}, \end{cases}$$

where  $\mathbf{0}_{p \times q}$  is the  $p \times q$  matrix of zeros. Note that  $\mathbf{I}_{p_1} - p_1^{-1} \mathbf{R} \mathbf{R}^\top$  and  $\mathbf{I}_{p_2} - p_2^{-1} \mathbf{C} \mathbf{C}^\top$  are orthogonal projection matrices with ranks  $p_1 - k_1$  and  $p_2 - k_2$ , respectively, and they are their own pseudoinverse matrices. Hence  $\mathbf{F}_t - p_2^{-1} \mathbf{X}_t \mathbf{C} = (\mathbf{I}_{p_1} - p_1^{-1} \mathbf{R} \mathbf{R}^\top) \mathbf{0}_{p_1 \times k_2} = \mathbf{0}_{p_1 \times k_2}$  and  $\mathbf{E}_t - p_1^{-1} \mathbf{X}_t^\top \mathbf{R} = (\mathbf{I}_{p_2} - p_2^{-1} \mathbf{C} \mathbf{C}^\top) \mathbf{0}_{p_2 \times k_1} = \mathbf{0}_{p_2 \times k_1}$  are the minimum norm solutions to the second and third linear systems, respectively (Ben-Israel and Greville, 2003). Then, by substituting  $\mathbf{F}_t = p_2^{-1} \mathbf{X}_t \mathbf{C}$  and  $\mathbf{E}_t = p_1^{-1} \mathbf{X}_t^\top \mathbf{R}$  into the first equation system, we derive the solution  $\mathbf{Z}_t = -(p_1 p_2)^{-1} \mathbf{R}^\top \mathbf{X}_t \mathbf{C}$ . Adopting the estimators of  $\mathbf{R}$  and  $\mathbf{C}$  in the last subsection, the factor matrices can be estimated by

$$\hat{\mathbf{F}}_t = \frac{\mathbf{X}_t \hat{\mathbf{C}}}{p_2}, \quad \hat{\mathbf{E}}_t = \frac{\mathbf{X}_t^\top \hat{\mathbf{R}}}{p_1}, \quad \hat{\mathbf{Z}}_t = -\frac{\hat{\mathbf{R}}^\top \mathbf{X}_t \hat{\mathbf{C}}}{p_1 p_2}. \quad (13)$$

Note that the global latent factor  $\hat{\mathbf{Z}}_t$  of RaDFaM is identical to  $\tilde{\mathbf{Z}}_t$  of BiMFaM up to sign. Accordingly, the estimated signal part of RaDFaM is

$$\hat{\mathbf{S}}_t = -\frac{\hat{\mathbf{R}} \hat{\mathbf{R}}^\top \mathbf{X}_t \hat{\mathbf{C}} \hat{\mathbf{C}}^\top}{p_1 p_2} + \frac{\hat{\mathbf{R}} \hat{\mathbf{R}}^\top \mathbf{X}_t}{p_1} + \frac{\mathbf{X}_t \hat{\mathbf{C}} \hat{\mathbf{C}}^\top}{p_2}. \quad (14)$$

### 3.3 Reconstruction Error Comparison

In this subsection, we compare the matrix reconstruction performance of RaDFaM and BiMFaM. We use a measure of performance used in image reconstruction because grayscale images can be represented by matrices; given a rectangular grid of pixels and a set of possible gray levels, a digital image can be represented by a matrix in which each entry represents a pixel gray value (i.e., brightness) ranging from 0 to 255 (Suetens, 2017).

For image data, a standard metric to measure the quality of reconstructed images compared with the original is the peak signal-to-noise ratio (PSNR) defined as

$$\text{PSNR} = 10 \log_{10} \left( \frac{\|\mathbf{X}\|_{\max}^2}{\|\mathbf{X} - \hat{\mathbf{X}}\|_F^2 / p_1 p_2} \right), \quad (15)$$

where  $\mathbf{X} = (\mathbf{X}_{ij}) \in \mathbb{R}^{p_1 \times p_2}$  is the original image,  $\hat{\mathbf{X}} = (\hat{\mathbf{X}}_{ij}) \in \mathbb{R}^{p_1 \times p_2}$  is the reconstructed image, and  $\|\mathbf{X}\|_{\max}$  is the maximum of the absolute value of entries in  $\mathbf{X}$ . The denominator inside the logarithm is the MSE  $:= \|\mathbf{X} - \hat{\mathbf{X}}\|_F^2 / p_1 p_2 = (p_1 p_2)^{-1} \sum_{i=1}^{p_1} \sum_{j=1}^{p_2} (\mathbf{X}_{ij} - \hat{\mathbf{X}}_{ij})^2$ . The more the reconstructed image resembles the original image, the smaller MSE will be and the larger PSNR will be (although this does not guarantee that viewers like the reconstructed image (Salomon, 2004)). PSNR is preferred to MSE because it is dimensionless and the logarithm in PSNR reduces the sensitivity to small variations in the reconstructed

image. Let  $\text{PSNR}_{t,RaD}(\text{MSE}_{t,RaD})$  and  $\text{PSNR}_{t,BiM}(\text{MSE}_{t,BiM})$  denote the PSNR (MSE) of RaDFaM and BiMFaM for the  $t$ th image, respectively, for  $t \in [T]$ . Then  $\widehat{\mathbf{X}}_t$  is  $\widehat{\mathbf{S}}_t$  in (14) for RaDFaM and  $\widetilde{\mathbf{S}}_t$  in (12) for BiMFaM. We have the following proposition.

**Proposition 3** *For each matrix observation  $\mathbf{X}_t$ ,  $t \in [T]$ , we have*

$$\text{PSNR}_{t,RaD} \geq \text{PSNR}_{t,BiM}. \quad (16)$$

or equivalently,

$$\text{MSE}_{t,RaD} \leq \text{MSE}_{t,BiM}. \quad (17)$$

Proposition 3 guarantees that the PSNR and MSE of RaDFaM are never worse than those of BiMFaM when both use spectral estimators of  $\mathbf{R}$  and  $\mathbf{C}$ . In addition, our numerical studies show that, even when other estimators (e.g. autoPCA, proPCA) are used for BiMFaM, RaDFaM still has better reconstruction error.

### 3.4 Algorithm and Factor Number Estimation

When the factor numbers  $k_1$  and  $k_2$  are known, the estimation algorithm is given in Algorithm 1.

---

#### Algorithm 1 RaDFaM

---

- 1: **Input:** matrix observations  $\{\mathbf{X}_t\}_{t=1}^T$ , factor numbers  $k_1$  and  $k_2$ .
- 2: compute the estimated loading matrices

$$\widehat{\mathbf{R}} = \sqrt{p_1} \text{eig}(\widehat{\mathbf{M}}_1, k_1) \text{ and } \widehat{\mathbf{C}} = \sqrt{p_2} \text{eig}(\widehat{\mathbf{M}}_2, k_2).$$

- 3: for  $t \in [T]$ , compute the estimated latent factor matrices and the signal part

$$\begin{aligned} \widehat{\mathbf{Z}}_t &= -\frac{\widehat{\mathbf{R}}^\top \mathbf{X}_t \widehat{\mathbf{C}}}{p_1 p_2}, \quad \widehat{\mathbf{F}}_t = \frac{\mathbf{X}_t \widehat{\mathbf{C}}}{p_2}, \quad \widehat{\mathbf{E}}_t = \frac{\mathbf{X}_t^\top \widehat{\mathbf{R}}}{p_1}, \\ \widehat{\mathbf{S}}_t &= -\frac{\widehat{\mathbf{R}} \widehat{\mathbf{R}}^\top \mathbf{X}_t \widehat{\mathbf{C}} \widehat{\mathbf{C}}^\top}{p_1 p_2} + \frac{\widehat{\mathbf{R}} \widehat{\mathbf{R}}^\top \mathbf{X}_t}{p_1} + \frac{\mathbf{X}_t \widehat{\mathbf{C}} \widehat{\mathbf{C}}^\top}{p_2}. \end{aligned}$$

- 4: **Output:**  $\widehat{\mathbf{R}}$ ,  $\widehat{\mathbf{C}}$ ,  $\{\widehat{\mathbf{Z}}_t\}_{t=1}^T$ ,  $\{\widehat{\mathbf{F}}_t\}_{t=1}^T$ ,  $\{\widehat{\mathbf{E}}_t\}_{t=1}^T$ , and  $\{\widehat{\mathbf{S}}_t\}_{t=1}^T$ .
- 

If  $k_1$  and  $k_2$  are unknown, we need to determine them before computing the spectral estimators. We adopt general ratio-type estimators for the factor numbers. Let  $\widehat{\lambda}_1(\widehat{\mathbf{M}}_1) \geq$

$\widehat{\lambda}_2(\widehat{\mathbf{M}}_1) \geq \dots \geq \widehat{\lambda}_{p_1}(\widehat{\mathbf{M}}_1) \geq 0$  denote the ordered eigenvalues of  $\widehat{\mathbf{M}}_1$  and let  $k_{\max}$  be a given upper bound for  $k_1$ . The number of factors can be estimated by

$$\widehat{k}_1 = \arg \max_{1 \leq j \leq k_{\max}} \frac{\widehat{\lambda}_j(\widehat{\mathbf{M}}_1)}{\widehat{\lambda}_{j+1}(\widehat{\mathbf{M}}_1)}, \quad (18)$$

and  $\widehat{k}_2$  can be defined similarly. This ratio-type estimator is widely used in factor models including the vector case and the matrix case (Lam and Yao, 2012; Yu et al., 2022). The consistency of the estimator is proved in the next section.

## 4 Asymptotic Properties

### 4.1 Assumptions

The theoretical results require assumptions which are similar to those made for BiMFaM (Chen and Fan, 2023; Yu et al., 2022). They can be regarded as extensions of those used in high-dimensional vector factor models (Stock and Watson, 2002; Bai, 2003).

**Assumption 1.**  *$\alpha$ -mixing: the vectorized factor processes  $\{\text{vec}(\mathbf{Z}_t)\}$ ,  $\{\text{vec}(\mathbf{F}_t)\}$ ,  $\{\text{vec}(\mathbf{E}_t)\}$ , and the noise process  $\{\text{vec}(\mathbf{e}_t)\}$  are  $\alpha$ -mixing.*

A vector process  $\{\mathbf{u}_t\}$  is  $\alpha$ -mixing, if  $\sum_{h=1}^{\infty} \alpha(h)^{1-2/\gamma} < \infty$  for some  $\gamma > 2$ , where  $\alpha(h) = \sup_i \sup_{A \in \mathcal{C}_{-\infty}^i, B \in \mathcal{C}_{i+h}^{\infty}} |P(A \cap B) - P(A)P(B)|$  with  $\mathcal{C}_i^j$  the  $\sigma$ -field generated by  $\{\mathbf{u}_t : i \leq t \leq j\}$ . The  $\alpha$ -mixing condition means that variables that are sufficiently far apart are asymptotic independent (Francq and Zakoian, 2019, Appendix A.3).

**Assumption 2** *Common factors: assume that  $k_1$  and  $k_2$  are fixed. For any  $t \in [T]$ ,  $i \in [p_1]$ ,  $j \in [p_2]$ ,  $u \in [k_1]$  and  $v \in [k_2]$ , there exists a positive constant  $m$  such that  $\mathbb{E}(\mathbf{Z}_{t,uv}^4) \leq m$ ,  $\mathbb{E}(\mathbf{F}_{t,iv}^8) \leq m$ ,  $\mathbb{E}(\mathbf{E}_{t,ju}^8) \leq m$  and*

$$\begin{aligned} \frac{1}{T} \sum_{t=1}^T \mathbf{Z}_t \mathbf{Z}_t^\top &\xrightarrow{a.s.} \boldsymbol{\Sigma}_{Z1}, \quad \frac{1}{T} \sum_{t=1}^T \mathbf{Z}_t^\top \mathbf{Z}_t \xrightarrow{a.s.} \boldsymbol{\Sigma}_{Z2}, \\ \frac{1}{Tp_1} \sum_{t=1}^T \mathbf{F}_t^\top \mathbf{F}_t &\xrightarrow{a.s.} \boldsymbol{\Sigma}_F, \quad \frac{1}{Tp_2} \sum_{t=1}^T \mathbf{E}_t^\top \mathbf{E}_t \xrightarrow{a.s.} \boldsymbol{\Sigma}_E, \end{aligned}$$

where  $\boldsymbol{\Sigma}_{Z1} \in \mathbb{R}^{k_1 \times k_1}$ ,  $\boldsymbol{\Sigma}_{Z2} \in \mathbb{R}^{k_2 \times k_2}$ ,  $\boldsymbol{\Sigma}_F \in \mathbb{R}^{k_2 \times k_2}$  and  $\boldsymbol{\Sigma}_E \in \mathbb{R}^{k_1 \times k_1}$  are positive definite matrices. Let  $\boldsymbol{\Sigma}_1 = \boldsymbol{\Sigma}_E + \boldsymbol{\Sigma}_{Z1}$  and  $\boldsymbol{\Sigma}_2 = \boldsymbol{\Sigma}_F + \boldsymbol{\Sigma}_{Z2}$ . Assume that  $\boldsymbol{\Sigma}_1$  and  $\boldsymbol{\Sigma}_2$  have spectral decompositions  $\boldsymbol{\Sigma}_1 = \boldsymbol{\Gamma}_1 \boldsymbol{\Lambda}_1 \boldsymbol{\Gamma}_1^\top$  and  $\boldsymbol{\Sigma}_2 = \boldsymbol{\Gamma}_2 \boldsymbol{\Lambda}_2 \boldsymbol{\Gamma}_2^\top$ , where the diagonal elements of  $\boldsymbol{\Lambda}_1$  and  $\boldsymbol{\Lambda}_2$  are distinct and arranged in decreasing order.

Assumption 2 requires the global factor matrix to have bounded fourth moments, and the row-wise and column-wise factor matrices to have bounded eighth moments. It also requires the second-order sample moments of the factor matrices to converge to positive definite matrices. (This can be derived under the  $\alpha$ -mixing Assumption 1, see (Athreya and Lahiri, 2006, Chapter 16) and (Francq and Zakoian, 2019, Appendix A.3.) for more details.) Finally, the assumption of distinct and decreasing eigenvalues of  $\Sigma_1$  and  $\Sigma_2$  results in unique eigen-decompositions and identifiable eigenvectors. Assumption 2 is an extension of the assumption in (Yu et al., 2022) with extra row-wise and column-wise factors.

**Assumption 3** *Loading matrices: there exist positive constants  $\bar{r}$  and  $\bar{c}$  such that  $\|\mathbf{R}\|_{\max} \leq \bar{r}$  and  $\|\mathbf{C}\|_{\max} \leq \bar{c}$ . As  $\min\{p_1, p_2\} \rightarrow \infty$ , we have  $\|p_1^{-1}\mathbf{R}^\top\mathbf{R} - \mathbf{I}_{k_1}\| \rightarrow 0$  and  $\|p_2^{-1}\mathbf{C}^\top\mathbf{C} - \mathbf{I}_{k_2}\| \rightarrow 0$ , where  $\|\cdot\|$  is the  $L_2$ -norm of a matrix.*

Assumption 3 is a model identification condition. It guarantees that our model belongs to the strong factor regime. This means that the factors are pervasively shared by entries of the observations, and the signal component has spiked eigenvalues relative to the noise component (Stock and Watson, 2002; Lam and Yao, 2011; Fan et al., 2013; Chen et al., 2020).

**Assumption 4** *Correlation: for any  $s, t \in [T], i \in [p_1], j \in [p_2], u \in [k_1]$  and  $v \in [k_2]$ , there exists a positive constant  $m$  such that*

$$(4.1) \quad \sum_{t_1=1}^T |\mathbb{E}(\mathbf{Z}_{t_1, u_1 v_1} \mathbf{Z}_{t_2, u_2 v_2})| \leq m.$$

$$(4.2) \quad \mathbb{E}(\mathbf{e}_{t, ij}^8) \leq m; \quad \sum_{t_1=1}^T \sum_{i_1=1}^{p_1} \sum_{j_1=1}^{p_2} |\mathbb{E}(\mathbf{e}_{t_1, i_1 j_1} \mathbf{e}_{t_2, i_2 j_2})| \leq m;$$

$$\sum_{t_1=1}^T \sum_{i_1, i_2=1}^{p_1} \sum_{j_1, j_2=1}^{p_2} |\text{cov}(\mathbf{e}_{t_1, i_1 j_1} \mathbf{e}_{t_1, i_2 j_2}, \mathbf{e}_{t_2, i_3 j_3} \mathbf{e}_{t_2, i_4 j_4})| \leq m;$$

$$\sum_{t_1=1}^T \sum_{i_1, i_2=1}^{p_1} \sum_{j_1, j_2=1}^{p_2} |\text{cov}(\mathbf{e}_{s, i_1 j_1} \mathbf{e}_{t_1, i_2 j_2}, \mathbf{e}_{s, i_3 j_3} \mathbf{e}_{t_2, i_4 j_4})| \leq m.$$

$$(4.3) \quad \sum_{t_1=1}^T \sum_{i_1=1}^{p_1} |\mathbb{E}(\mathbf{F}_{t_1, i_1 v_1} \mathbf{F}_{t_2, i_2 v_2})| \leq m; \quad \sum_{t_1=1}^T \sum_{i_1, i_2=1}^{p_1} |\text{cov}(\mathbf{F}_{t_1, i_1 v_1} \mathbf{F}_{t_1, i_2 v_2}, \mathbf{F}_{t_2, i_3 v_3} \mathbf{F}_{t_2, i_4 v_4})| \leq m;$$

$$\sum_{t_1=1}^T \sum_{i_1, i_2=1}^{p_1} |\text{cov}(\mathbf{F}_{s, i_1 v_1} \mathbf{F}_{t_1, i_2 v_2}, \mathbf{F}_{s, i_3 v_3} \mathbf{F}_{t_2, i_4 v_4})| \leq m.$$

$$(4.4) \quad \sum_{t_1=1}^T \sum_{j_1=1}^{p_2} |\mathbb{E}(\mathbf{E}_{t_1, j_1 u_1} \mathbf{E}_{t_2, j_2 u_2})| \leq m; \quad \sum_{t_1=1}^T \sum_{j_1, j_2=1}^{p_2} |\text{cov}(\mathbf{E}_{t_1, j_1 u_1} \mathbf{E}_{t_1, j_2 u_2}, \mathbf{E}_{t_2, j_3 u_3} \mathbf{E}_{t_2, j_4 u_4})| \leq m;$$

$$\sum_{t_1=1}^T \sum_{j_1, j_2=1}^{p_2} |\text{cov}(\mathbf{E}_{s, j_1 u_1} \mathbf{E}_{t_1, j_2 u_2}, \mathbf{E}_{s, j_3 u_3} \mathbf{E}_{t_2, j_4 u_4})| \leq m.$$

Assumption 4 focuses on the cross-sectional and temporal correlation of the noise matrices  $\mathbf{e}_t$  and the factor matrices  $\mathbf{Z}_t$ ,  $\mathbf{F}_t$  and  $\mathbf{E}_t$ . Assumption 4.1 requires the temporal correlation of  $\mathbf{Z}_t$  to be weak, and no constraint is put on the cross-sectional correlation  $\mathbf{Z}_t$  due to the finiteness of  $k_1$  and  $k_2$ . Similar to Assumption 4.1, Assumptions 4.2-4.4 are made for  $\mathbf{e}_t$ ,  $\mathbf{F}_t$  and  $\mathbf{E}_t$ , respectively. Taking Assumption 4.2 of the matrix noise as an example, it requires bounded eighth moment for each element; its cross-sectional and temporal correlation is required to be weak; its cross-sectional and temporal correlation of  $\mathbf{e}_t \circ \mathbf{e}_t \in \mathbb{R}^{p_1 \times p_2 \times p_1 \times p_2}$  and  $\mathbf{e}_s \circ \mathbf{e}_t \in \mathbb{R}^{p_1 \times p_2 \times p_1 \times p_2}$  is required to be weak, where  $\circ$  is the outer product. In summary, we assume the correlations in the noise part and the factors are weak, and the independent matrix observations satisfy Assumption 4.

**Assumption 5** *Central limit theorems:*

1. for  $i \in [p_1]$ ,

$$\frac{1}{\sqrt{T}} \sum_{t=1}^T \mathbf{Z}_t \mathbf{F}_{t,i} \xrightarrow{d} N(\mathbf{0}, \mathbf{V}_{1i}), \quad \text{where } \mathbf{V}_{1i} = \lim_{T \rightarrow \infty} \frac{1}{T} \sum_{s,t} \mathbb{E}(\mathbf{Z}_t \mathbf{F}_{t,i} \mathbf{F}_{s,i}^\top \mathbf{Z}_s^\top);$$

2. for  $j \in [p_2]$ ,

$$\frac{1}{\sqrt{T}} \sum_{t=1}^T \mathbf{Z}_t^\top \mathbf{E}_{t,j} \xrightarrow{d} N(\mathbf{0}, \mathbf{V}_{2j}), \quad \text{where } \mathbf{V}_{2j} = \lim_{T \rightarrow \infty} \frac{1}{T} \sum_{s,t} \mathbb{E}(\mathbf{Z}_t^\top \mathbf{E}_{t,j} \mathbf{E}_{s,j}^\top \mathbf{Z}_s^\top).$$

Assumption 5 is useful when deriving the asymptotic distributions of the estimated loading matrices. Under Assumptions 1-4, Assumption 5 can be derived by applying the central limit theorem for  $\alpha$ -mixing processes (Athreya and Lahiri (2006); Francq and Zakoian (2019)). Assumption 5 is different from the corresponding condition for BiMFaM in that the main terms differ due to the incorporation of row-wise and column-wise factors.

## 4.2 Asymptotic Properties

Assumption 3 only ensures uniqueness of the column space up to an orthogonal rotation, so we prove that there exist asymptotic orthogonal matrices  $\mathbf{H}_1$  and  $\mathbf{H}_2$  such that  $\hat{\mathbf{R}}$  is a consistent estimator of  $\mathbf{R}\mathbf{H}_1$ , and  $\hat{\mathbf{C}}$  is a consistent estimator of  $\mathbf{C}\mathbf{H}_2$ . Then the convergence rates of  $\hat{\mathbf{R}}$  and  $\hat{\mathbf{C}}$  in the Frobenius norm are given in Theorem 1.

**Theorem 1** *Suppose that  $T$ ,  $p_1$  and  $p_2$  tend to infinity, and that  $k_1$  and  $k_2$  are fixed. If Assumptions 1-4 hold, then there exist asymptotic orthogonal matrices  $\mathbf{H}_1$  and  $\mathbf{H}_2$  such*

that

$$\frac{1}{p_1} \|\widehat{\mathbf{R}} - \mathbf{R}\mathbf{H}_1\|_F^2 = O_p\left(\frac{1}{T} + \frac{1}{p_1^2}\right), \text{ and } \frac{1}{p_2} \|\widehat{\mathbf{C}} - \mathbf{C}\mathbf{H}_2\|_F^2 = O_p\left(\frac{1}{T} + \frac{1}{p_2^2}\right).$$

The convergence rate of  $\widehat{\mathbf{R}}$  ( $\widehat{\mathbf{C}}$ ) in Theorem 1 is the same as in the high-dimensional vector factor models of Bai (2003) with  $T$  samples of size  $p_1$  or  $p_2$ . For BiMFaM, the convergence rates of the autoPCA estimators in Wang et al. (2019) are  $O_p(\frac{1}{T})$ , and the convergence rates for  $\alpha$ -PCA estimators are  $O_p(\frac{1}{Tp_2} + \frac{1}{p_1^2})$  and  $O_p(\frac{1}{Tp_1} + \frac{1}{p_2^2})$ . These latter rates are identical to those in vector factor models with  $Tp_2$  or  $Tp_1$  samples of size  $p_1$  or  $p_2$  (Yu et al., 2022). Hence, RaDFaM improves the reconstruction performance at the cost of a slower convergence rate when  $Tp_2 = o(p_1^2)$  and  $Tp_1 = o(p_2^2)$ . The difference is due to the incorporation of row and column effects in addition to their interactions.

We can also derive the asymptotic distribution of the estimated loading matrices. As the row sizes of  $\mathbf{R}$  and  $\mathbf{C}$  tend to infinity, we establish the row-wise asymptotic distribution in the following Theorem 2.

**Theorem 2** *Suppose that  $T$ ,  $p_1$  and  $p_2$  tend to infinity, and that  $k_1$  and  $k_2$  are fixed. If Assumptions 1-5 hold, then*

1. *for  $i \in [p_1]$ , we have*

$$\begin{cases} \sqrt{T}(\widehat{\mathbf{R}}_{i\cdot} - \mathbf{H}_1^\top \mathbf{R}_{i\cdot}) \xrightarrow{d} N(\mathbf{0}, \mathbf{\Lambda}_1^{-1} \mathbf{\Gamma}_1^\top \mathbf{V}_{1i} \mathbf{\Gamma}_1 \mathbf{\Lambda}_1^{-1}), & T = o(p_1^2), \\ \widehat{\mathbf{R}}_{i\cdot} - \mathbf{H}_1^\top \mathbf{R}_{i\cdot} = O_p(\frac{1}{p_1}), & p_1^2 = O(T); \end{cases}$$

2. *for  $j \in [p_2]$ , we have*

$$\begin{cases} \sqrt{T}(\widehat{\mathbf{C}}_{j\cdot} - \mathbf{H}_2^\top \mathbf{C}_{j\cdot}) \xrightarrow{d} N(\mathbf{0}, \mathbf{\Lambda}_2^{-1} \mathbf{\Gamma}_2^\top \mathbf{V}_{2j} \mathbf{\Gamma}_2 \mathbf{\Lambda}_2^{-1}), & T = o(p_2^2), \\ \widehat{\mathbf{C}}_{j\cdot} - \mathbf{H}_2^\top \mathbf{C}_{j\cdot} = O_p(\frac{1}{p_2}), & p_2^2 = O(T). \end{cases}$$

Theorem 2 shows that the estimated loading matrix can be asymptotically normal when  $p_1$  and  $p_2$  are sufficiently large. Even if the central limit theorem does not hold, regardless of the limiting relationship between  $T$  and  $\{p_d\}_{d=1}^2$ , the estimated loading matrices are still consistent.

We now turn to the consistency of the estimated signal component. As the size of  $\mathbf{S}_t$  tends to infinity, we will prove its element-wise consistency. The  $(i, j)$ th elements of  $\mathbf{S}_t$  and  $\widehat{\mathbf{S}}_t = \widehat{\mathbf{X}}_t$  are

$$\mathbf{S}_{t,ij} = \mathbf{R}_{i\cdot}^\top \mathbf{Z}_t \mathbf{C}_{j\cdot} + \mathbf{R}_{i\cdot}^\top \mathbf{E}_{t,j\cdot} + \mathbf{F}_{t,i\cdot}^\top \mathbf{C}_{j\cdot} \quad \text{and} \quad \widehat{\mathbf{S}}_{t,ij} = \widehat{\mathbf{R}}_{i\cdot}^\top \widehat{\mathbf{Z}}_t \widehat{\mathbf{C}}_{j\cdot} + \widehat{\mathbf{R}}_{i\cdot}^\top \widehat{\mathbf{E}}_{t,j\cdot} + \widehat{\mathbf{F}}_{t,i\cdot}^\top \widehat{\mathbf{C}}_{j\cdot},$$

respectively.



**Theorem 3** *Suppose that  $k_1$  and  $k_2$  are fixed, and that  $T$ ,  $p_1$  and  $p_2$  tend to infinity. If Assumptions 1-4 hold, then we have*

$$|\widehat{\mathbf{S}}_{t,ij} - \mathbf{S}_{t,ij}| = O_p\left(\frac{1}{\sqrt{T}} + \frac{1}{\sqrt{p_1}} + \frac{1}{\sqrt{p_2}}\right).$$

Similar to the convergence rates of the estimators of the loading matrices, the convergence rate of the estimator of the signal component in RaDFaM is slower than that in BiMFaM. However, as shown in Proposition 3, RaDFaM has better reconstruction performance.

Theorems 1-3 are proved with fixed factor numbers  $k_1$  and  $k_2$ . If the factor numbers are unknown, the ratio-type estimator (18) provides consistent estimators.

**Theorem 4** *Suppose that  $k_1$  and  $k_2$  are fixed, and that  $T$ ,  $p_1$  and  $p_2$  tend to infinity. If Assumptions 1-4 hold, then we have*

$$P(\widehat{k}_1 \neq k_1) \rightarrow 0 \quad \text{and} \quad P(\widehat{k}_2 \neq k_2) \rightarrow 0.$$

Theorem 4 shows that with large enough  $k_{max}$ , the factor numbers can be estimated consistently. The proof can be done by following the arguments similar to those in the proof of Lemma 1 given in the online supplement. Our estimator has the same form as the initial estimator in Yu et al. (2022) and the  $\alpha$ -PCA estimator in Chen and Fan (2023) with  $\alpha = 0$ , so the ratio-type estimator provides the same estimates of the factor numbers for RaDFaM and BiMFaM.

## 5 Numerical Studies

In this section, we present simulations to compare the finite sample performance of the proposed RaDFaM. The simulation settings for four different simulation scenarios are introduced in Subsection 5.1, and the performance measures are presented in Subsection 5.2. Simulation results assessing the consistency of the loading matrices, the performance of the signal components estimators and matrix reconstruction, and the asymptotic normality of the loading matrices estimators are reported in Subsection 5.3.

### 5.1 Simulation Settings

The simulation data is generated with factor numbers  $k_1 = k_2 = 3$  and 6 sets of  $(T, p_1, p_2)$ , which are (20, 50, 100), (20, 100, 100), (50, 20, 50), (50, 100, 100), (100, 20, 50) and (100, 50, 100).

The loading matrix  $\mathbf{R}$  is taken as  $\sqrt{p_1}$  times the matrix of the first  $k_1$  left singular vectors of the SVD decomposition of a  $p_1 \times k_1$ -dimensional matrix with independent standard normal elements, and the loading matrix  $\mathbf{C}$  is generated similarly. We then generate  $\mathbf{Z}_t$ ,  $\mathbf{E}_t$  and  $\mathbf{F}_t$  using the following vector auto-regression models

$$\begin{aligned}\text{vec}(\mathbf{Z}_t) &= \phi \text{vec}(\mathbf{Z}_{t-1}) + \sqrt{1 - \phi^2} \mathbf{u}_t, \\ \text{vec}(\mathbf{F}_t) &= \psi \text{vec}(\mathbf{F}_{t-1}) + \sqrt{1 - \psi^2} \boldsymbol{\xi}_t, \\ \text{vec}(\mathbf{E}_t) &= \gamma \text{vec}(\mathbf{E}_{t-1}) + \sqrt{1 - \gamma^2} \boldsymbol{\eta}_t,\end{aligned}$$

where  $\mathbf{u}_t \sim N(\mathbf{0}, \mathbf{I}_{k_1 k_2})$ ,  $\boldsymbol{\xi}_t \sim N(\mathbf{0}, \mathbf{I}_{p_1 k_2})$ ,  $\boldsymbol{\eta}_t \sim N(\mathbf{0}, \mathbf{I}_{p_2 k_1})$ , and the entries of the initial values of  $\text{vec}(\mathbf{Z}_t)$ ,  $\text{vec}(\mathbf{F}_t)$  and  $\text{vec}(\mathbf{E}_t)$  are standard normal. The coefficients  $\phi$ ,  $\psi$  and  $\gamma$  control the temporal correlation of the factor matrices. Last, we generate  $\mathbf{e}_t \sim MN(\mathbf{0}; \boldsymbol{\Omega}_e, \boldsymbol{\Delta}_e)$ , where  $\boldsymbol{\Omega}_e$  and  $\boldsymbol{\Delta}_e$  both have 1's on the diagonal and constant off-diagonal elements  $1/p_1$  and  $1/p_2$ , respectively. We consider four different scenarios.

**Scenario I:** (Uncorrelated & RaDFaM)  $(\phi, \psi, \gamma) = (0, 0, 0)$ , so the factor matrix series are temporally uncorrelated, and data are generated from RaDFaM (3).

**Scenario II:** (Uncorrelated & BiMFaM)  $(\phi, \psi, \gamma) = (0, 0, 0)$ , so the factor matrix series are temporally uncorrelated, and data are generated from BiMFaM, i.e., only including the bilinear part.

**Scenario III:** (Correlated & RaDFaM)  $(\phi, \psi, \gamma) = (0.6, 0.8, 0.8)$ , so the factor matrix series are temporally correlated, and data are generated from RaDFaM (3).

**Scenario IV:** (Correlated & BiMFaM)  $(\phi, \psi, \gamma) = (0.6, 0.8, 0.8)$ , so the factor matrix series are temporally correlated, and data are generated from BiMFaM.

We name our estimation procedure as sPCA, since it relies on the separable covariance structure. We compare estimates of the loading matrices, the signal component, and the reconstruction error obtained using sPCA for RaDFaM, autoPCA (Wang et al., 2019),  $\alpha$ -PCA with  $\alpha = 0$  (Chen and Fan, 2023), and proPCA for BiMFaM (Yu et al., 2022).

## 5.2 Performance Measures

For the estimators of the loading matrices, we use

$$\begin{aligned}\mathcal{D}(\hat{\mathbf{R}}, \mathbf{R}) &= \|\hat{\mathbf{R}}(\hat{\mathbf{R}}^\top \hat{\mathbf{R}})^{-1} \hat{\mathbf{R}}^\top - \mathbf{R}(\mathbf{R}^\top \mathbf{R})^{-1} \mathbf{R}^\top\|_2, \\ \mathcal{D}(\hat{\mathbf{C}}, \mathbf{C}) &= \|\hat{\mathbf{C}}(\hat{\mathbf{C}}^\top \hat{\mathbf{C}})^{-1} \hat{\mathbf{C}}^\top - \mathbf{C}(\mathbf{C}^\top \mathbf{C})^{-1} \mathbf{C}^\top\|_2,\end{aligned}$$

to characterize the distance between the estimated and the true column space. For the estimator of the signal part, we use

$$\mathcal{D}_{signal} = \sqrt{\frac{1}{Tp_1p_2} \sum_{t=1}^T \|\hat{\mathbf{S}}_t - \mathbf{S}_t\|_F^2},$$

to gauge its distance with the true signal. For the reconstruction error, we use

$$\text{RMSE} = \sqrt{\frac{1}{T} \sum_{t=1}^T \text{MSE}_t}, \quad \overline{\text{PSNR}} = \frac{1}{T} \sum_{t=1}^T \text{PSNR}_t,$$

as performance measures, where  $\text{MSE}_t$  and  $\text{PSNR}_t$  are defined in Section 3.3.

### 5.3 Simulation Results

To compare the row-wise loading matrix estimators, boxplots of  $\mathcal{D}(\hat{\mathbf{R}}, \mathbf{R})$  from 100 replications of the four different methods are reported in Figure 2. We see that autoPCA performs poorly because it is not applicable to these scenarios (uncorrelated observations or correlated errors). Since  $\alpha$ -PCA with  $\alpha = -1$  and sPCA for loading matrices are identical, regardless of the generating model, they have the same results under all four scenarios. proPCA performs worse than  $\alpha$ -PCA and sPCA in Scenarios I and III, and better in Scenarios II and IV, which agrees with the results in Yu et al. (2022). The results for column-wise loading matrix estimators are similar; see the online supplement.

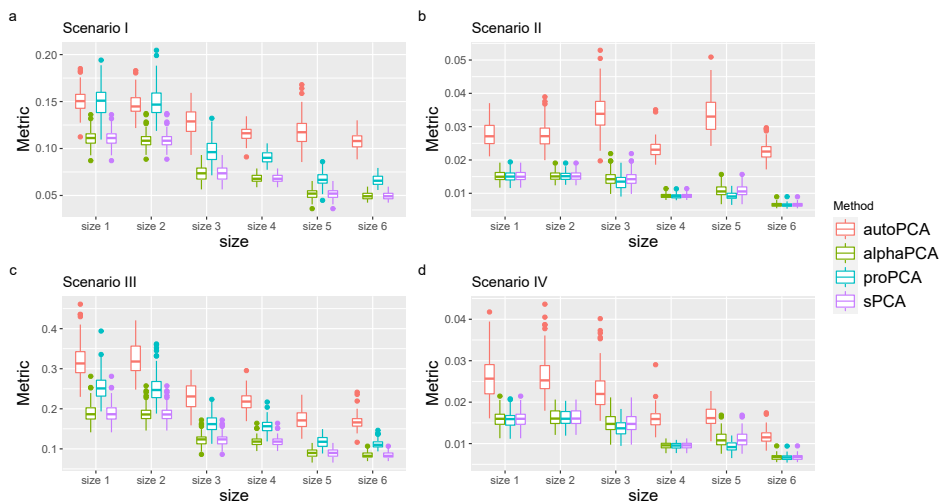


Figure 2: Boxplots of  $\mathcal{D}(\hat{\mathbf{R}}, \mathbf{R})$  for four estimation methods under six size settings in four scenarios.

To assess the performance of signal components estimators and matrix reconstruction for the four methods, boxplots of  $\mathcal{D}_{signal}$ , RMSE and  $\overline{\text{PSNR}}$  from 100 replications are shown in Figures 3 - 5. Although the estimated signal components of sPCA performs poorer than the other methods when the data are generated from BiMFaM (Scenarios II and IV in Figure 3), its matrix reconstruction performance is better than the other methods for both generating models (all scenarios in Figures 4 and 5).

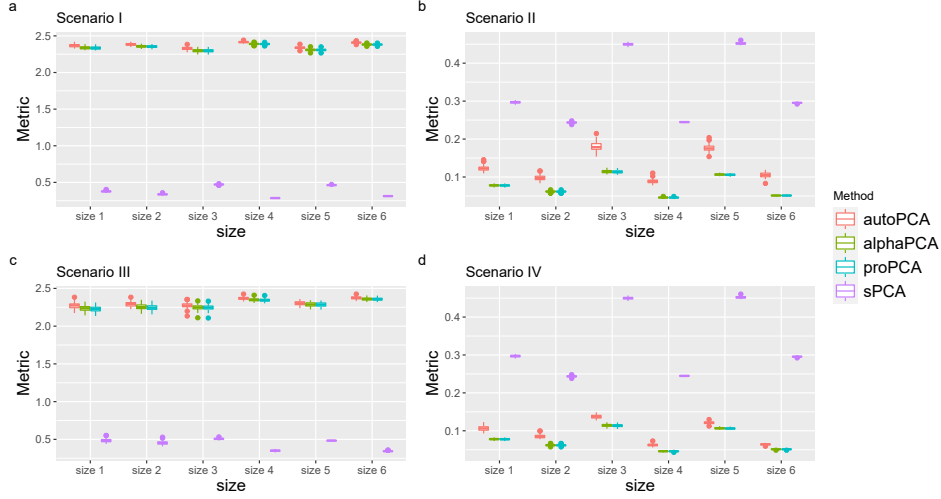


Figure 3: Boxplots of  $\mathcal{D}_{signal}$  for four estimation methods under six size settings in four scenarios.

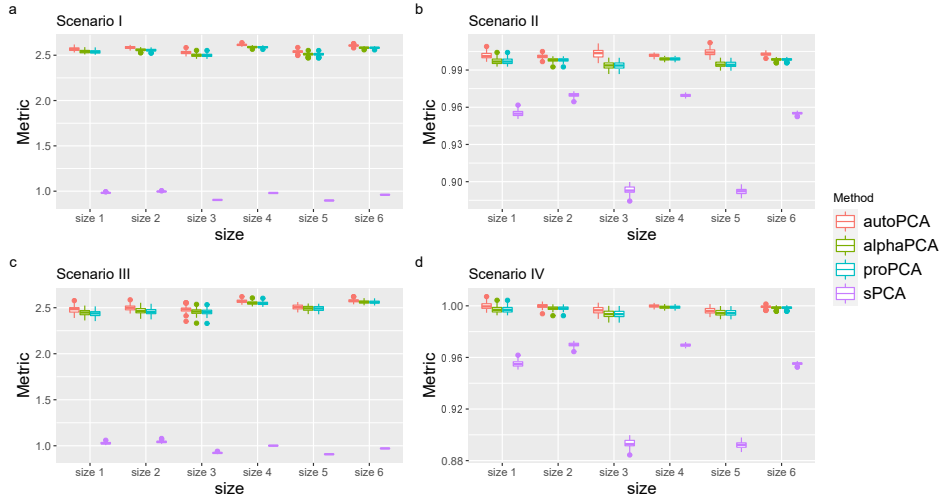


Figure 4: Boxplots of RMSE for four estimation methods under six size settings in four scenarios.

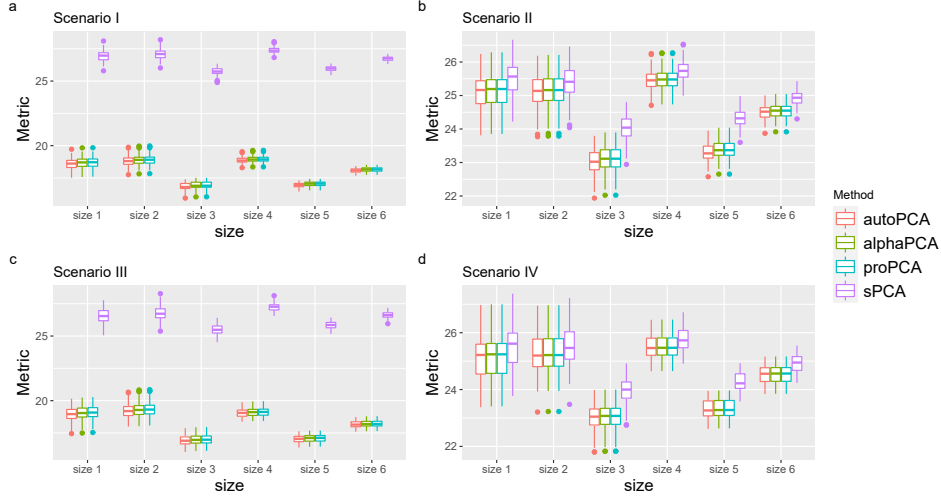


Figure 5: Boxplots of  $\overline{\text{PSNR}}$  for four estimation methods under six size settings in four scenarios.

We illustrate the asymptotic normality of the sPCA estimator  $\hat{\mathbf{R}}$  under Scenario I with  $(T, p_1, p_2) = (100, 150, 150)$ . In this case, the asymptotic covariance matrix of  $\hat{\mathbf{R}}_i$  is  $k_2/(k_2 + 1)^2 \mathbf{I}_{k_1}$ , so we present the histogram and QQ plot of the third element of  $(k_2 + 1)\sqrt{T/k_2}(\hat{\mathbf{R}}_1 - \mathbf{H}_1^\top \mathbf{R}_1)$  over 1000 replications in Figure 6. The smooth curve in the left plot is the probability density function of the standard normal distribution, and the QQ plot supports the normal approximation (the  $p$ -value of the Shapiro-Wilk test for normality is 0.4276).

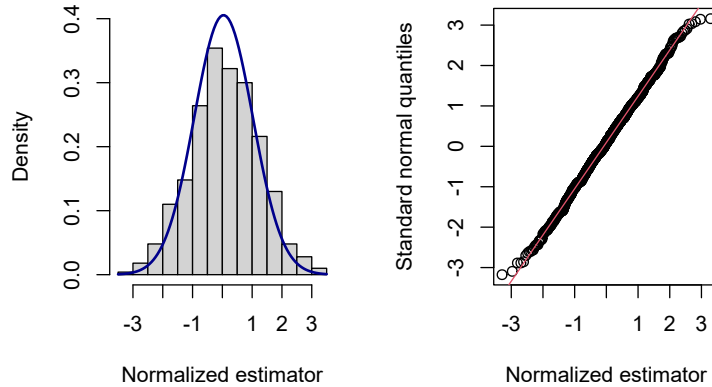


Figure 6: Histogram (with superimposed standard normal density) and QQ-plot of the normalised estimator  $\hat{\mathbf{R}}_{13}$ .

## 6 Real Data Analysis

### 6.1 Independent Dataset: CT Images for COVID-19

Nucleic acid detection, antibody detection via blood testing and computed tomography (CT) imaging are the most common tests for detecting COVID-19. Early in the COVID-19 pandemic, due to the shortage of test kits, CT and other chest imaging techniques were important for diagnosing COVID-19 (Yang et al., 2020). As discussed in Subsection 3.3, grayscale image data can be regarded as matrix data. In this subsection, we apply the proposed method to the COVID-CT dataset collected by Yang et al. (2020), which contains 714 CT chest images showing COVID-19 with values between 0 and 1. Each image has been resized to  $150 \times 150$ , so  $T = 714$ ,  $p_1 = 150$  and  $p_2 = 150$ .

**Image reconstruction: RaDFaM vs BiMFaM** Both BiMFaM and RaDFaM can be used to extract low-dimensional features from the observations, and the estimated low-rank signal component can be regarded as the reconstruction of the original image. As we said, though RaDFaM loses some sufficiency in dimension reduction, the intensity of the signal component is strengthened due to the mode-wise latent factor matrices without additional computation cost. To illustrate this point, we compare the reconstruction performance of four PCA type methods, i.e., autoPCA,  $\alpha$ -PCA, proPCA for BiMFaM, and sPCA for RaDFaM, with varying factor numbers of  $k_1 = k_2 = \{5, 15, 25, 35, 45\}$ .

The results of RMSE and  $\overline{\text{PSNR}}$  are shown in the first four rows of Tables 1 and 2, respectively. Upon examining the results, it is evident that the performance of all PCA type methods improves as the number of factors increases. It is noteworthy that sPCA outperforms the other methods for all the factor numbers tested. These findings suggest that increasing the number of factors could be a useful strategy to enhance the performance of the methods under consideration, with sPCA being the most effective approach among them.

In addition, we also tried the refined TCPD method (Chang et al., 2023) with time lag  $K = 1$ , CP rank  $d = 1$ , and randomly selected linear combination. The RMSE and  $\overline{\text{PSNR}}$  results are 0.3339 and 9.8321, respectively. The results indicate that while the TCPD method may achieve more effective data compression, its reconstruction performance is comparatively suboptimal.

**Image reconstruction: RaDFaM vs Deep learning** We also utilize the autoencoder (AE) method to compare the reconstruction performance of the proposed method

with deep learning approaches (Hinton and Salakhutdinov, 2006; Fan et al., 2021). The number of hidden layers are set to be 1 for AE-1, and 5 for AE-5 with the latent feature dimensions of  $k_1$  and  $(256, 128, k_1, 128, 256)$ , respectively, where  $k_1$  is the number of row factors in the statistical methods. We use the whole sample as the batch, and carry out 500 epochs. In addition, to fully make use of the matrix structure information, a convolutional autoencoder (CAE) of 8 hidden layers with  $k_1$  neurons in the central fully connected bottleneck layer is used (Guo et al., 2017). We take 32 as the batch size, and carry out 50 epochs.

The results of RMSE and  $\overline{\text{PSNR}}$  are shown in the last three rows of Tables 1 and 2, respectively. According to the results, all PCA-based methods performance better than the AE and CAE approaches. This could be attributed to the relatively small size of the data sample, which may not be adequate for the deep learning methods to operate effectively. Additionally, the vectorized image input may result in the loss of structural information. Conversely, matrix factor models have significantly fewer parameters and directly adopt the matrix structure. This may explain their superior performance in this case.

Table 1: RMSEs of different estimation methods for different choices of  $(k_1, k_2)$  applied to the COVID-CT data.

Model	Method/ $(k_1, k_2)$	(5, 5)	(15, 15)	(25, 25)	(35, 35)	(45, 45)
BiMFaM	autoPCA	0.2009	0.1347	0.1097	0.0949	0.0836
	$\alpha$ -PCA	0.1907	0.1238	0.0976	0.0814	0.0698
	proPCA	0.1899	0.1230	0.0969	0.0810	0.0695
RaDFaM	sPCA	<b>0.1246</b>	<b>0.0782</b>	<b>0.0579</b>	<b>0.0456</b>	<b>0.0369</b>
AE	AE-1	0.3403	0.3403	0.3403	0.3404	0.3404
	AE-5	0.3403	0.3403	0.3403	0.3403	0.3403
	CAE	0.3383	0.3383	0.3383	0.3384	0.3384

Table 2:  $\overline{\text{PSNRs}}$  of different estimation methods for different choices of  $(k_1, k_2)$  applied to the COVID-CT data.

Model	Method/ $(k_1, k_2)$	(5, 5)	(15, 15)	(25, 25)	(35, 35)	(45, 45)
BiMFaM	autoPCA	14.1498	17.6611	19.4595	20.7566	21.9110
	$\alpha$ -PCA	14.6213	18.3889	20.5233	22.1957	23.6577
	proPCA	14.6597	18.4334	20.5756	22.2437	23.6945
RaDFaM	sPCA	<b>18.3016</b>	<b>22.4788</b>	<b>25.3164</b>	<b>27.6773</b>	<b>29.8249</b>
AE	AE-1	9.5018	9.5010	9.5005	9.4994	9.4976
	AE-5	9.5023	9.5022	9.5019	9.5020	9.5020
	CAE	9.5534	9.5537	9.5518	9.5516	9.5499

**Image classification: RaDFaM vs BiMFaM** The extracted latent factor matrices from the matrix factor models can be used as input and instrumental variables in models for downstream data analyses (Chen et al., 2022). Let  $Y_t \in \{0, 1\}$  be the label of the  $t$ -th CT image with 1 for the positive scan and 0 for the negative scan. To classify the COVID-CT data, based on RaDFaM, the following hierarchical logistic regression model ( $\text{HLR}_{RaD}$ ) can be established

$$\begin{cases} \text{logit}P(Y_t = 1 | \mathbf{Z}_t, \mathbf{F}_t, \mathbf{E}_t) = \gamma + \langle \mathbf{B}_1, \mathbf{Z}_t \rangle + \langle \mathbf{B}_2, \mathbf{F}_t \rangle + \langle \mathbf{B}_3, \mathbf{E}_t \rangle \\ \mathbf{X}_t = \mathbf{R}\mathbf{Z}_t\mathbf{C}^\top + \mathbf{R}\mathbf{E}_t^\top + \mathbf{F}_t\mathbf{C}^\top + \mathbf{e}_t, \end{cases}$$

where  $\gamma$  is the intercept,  $\mathbf{B}_1 \in \mathbb{R}^{k_1 \times k_2}$ ,  $\mathbf{B}_2 \in \mathbb{R}^{p_1 \times k_2}$  and  $\mathbf{B}_3 \in \mathbb{R}^{p_2 \times k_1}$  are the regression coefficients, and  $\langle \cdot, \cdot \rangle$  is the inner product operation. For BiMFaM based HLR ( $\text{HLR}_{BiM}$ ), the last two terms in the logistic regression are omitted. To compared the classification performance of  $\text{HLR}_{RaD}$  and  $\text{HLR}_{BiM}$ , we randomly split the samples into a training set (80%) and a testing set (20%). In the first step of the training part, the RaDFaM and BiMFaM are fitted on the training set, yielding  $\hat{\mathbf{R}}$ ,  $\hat{\mathbf{C}}$ ,  $\hat{\mathbf{Z}}_t^{train}$ ,  $\hat{\mathbf{F}}_t^{train}$  and  $\hat{\mathbf{E}}_t^{train}$ . In the second step of the training part, the logistic regression is fitted and yielding the estimated regression coefficient. For the testing part, the  $\hat{\mathbf{Z}}_t^{test}$ ,  $\hat{\mathbf{F}}_t^{test}$  and  $\hat{\mathbf{E}}_t^{test}$  are obtained by the factor score equations, and then the prediction can be obtained from the regression. The procedure is repeated randomly 100 times. For the choice of factor numbers, the ratio-type estimator results in  $(\hat{k}_1, \hat{k}_2) = (1, 1)$ . For illustration, varying factor numbers  $k_1 = k_2 \in \{1, 2, 3, 4, 5\}$  are choosen. LASSO type thresholding is adopted for sPCA as the vectorized latent factor matrices  $(\text{vec}^\top(\mathbf{Z}_t), \text{vec}^\top(\mathbf{F}_t), \text{vec}^\top(\mathbf{E}_t))^\top$  may be high-dimensional



with the increasing number of factors. The average AUC values of  $\text{HLR}_{BiM}$  with  $\alpha$ -PCA, proPCA, and  $\text{HLR}_{RaD}$  with sPCA are shown in Figure 7, we can see that the classification performance improves with the increasing number of factors, and  $\text{HLR}_{RaD}$  with sPCA (the black triangle line) has better performance, especially with a small number of factors.

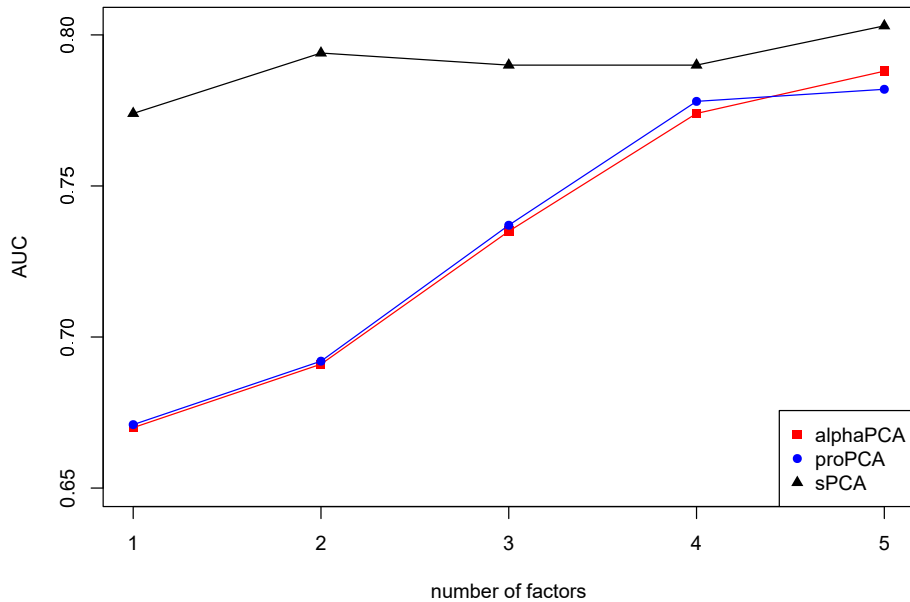


Figure 7: Average AUC values of three different methods for different choice of  $(k_1, k_2)$  applied to COVID-CT data.

## 6.2 Time Series: Multinational Macroeconomic Indices

We next analyze the multinational macroeconomic indices data set mentioned in the introduction. It contains 10 quarterly macroeconomic indices from 14 countries (United States of America, Canada, New Zealand, Australia, Norway, Ireland, Denmark, United Kingdom, Finland, Sweden, France, Netherlands, Austria and Germany) for the 74 quarters from 2000.Q1 to 2018.Q2. The indices consist of four groups: the production group (P:TIEC, P:TM, GDP), the consumer price group (CPI:FOOD, CPI:ENER, CPI:TOT), the money market group (IR:Long, IR:SHORT), and the international trade group (IT:EXP, IT:IM). The country abbreviations are given in Appendix G of the online supplement.

The data have been preprocessed using methods similar to those in Chen and Fan (2023). For the production and international trade groups, the univariate time series are

transformed by taking the first difference of the logarithm of the series. For the consumer price group, the univariate time series are transformed by taking the second difference of the logarithm of the series. For the money market group, the univariate time series are transformed by taking the first difference of the series. Hence, after centering the matrix-variate series to eliminate mean effects, we have observations with  $T = 72$ ,  $p_1 = 14$  and  $p_2 = 10$ . We apply autoPCA,  $\alpha$ -PCA, proPCA for BiMFaM, and sPCA for RaDFaM to the data.

**Clustering** For the factor numbers, we choose  $k_1 = 3$  and  $k_2 = 4$ . For interpretability, we apply the varimax rotation to the loading matrices, multiply the rotated loadings by 30, and then truncate these to integer values. The tables of estimated loading matrices are given in Appendix G of the online supplement, and the hierarchical clustering results based on the rotated estimated loading matrices are shown in Figures 8 and 9. For the row factors, the results of the  $\alpha$ -PCA and sPCA methods are identical, but are different from those of the autoPCA and proPCA methods. All the methods cluster the United States of America, Canada and New Zealand into one group. For the column factors, proPCA gives the most similar clustering to the true index groups, followed closely by  $\alpha$ -PCA and sPCA.

**Reconstruction comparison in terms of correlation effects** To illustrate the effect of the additional row and column information contained in RaDFaM, we compare the signal components obtained from RaDFaM and BiMFaM. We compute the row-wise, column-wise, and the interaction between rows and columns correlation of the estimated signal components for BiMFaM (autoPCA,  $\alpha$ -PCA and proPCA) and RaDFaM (sPCA). We evaluate their performance through heatmaps of the difference between these estimated correlations and the observed correlation in the original data (Figures 1). The results in Figure 10 show that the pattern of row-wise, column-wise, and the interaction between rows and columns correlation for RaDFaM is closer to the observed correlations (much lighter in color). This result together with Proposition 3 explain why it is important to include the pure row-wise and column-wise parts in RaDFaM to achieve better reconstruction performance.

**Reconstruction comparison in terms of RMSE** We use 10 fold cross-validation to evaluate the difference between the observed and estimated matrices in terms of RMSE for different values of factor numbers. The TCPD method with PCA-type linear combination gave a RMSE of 0.38019; the results shown in Table 3 show that our method performs

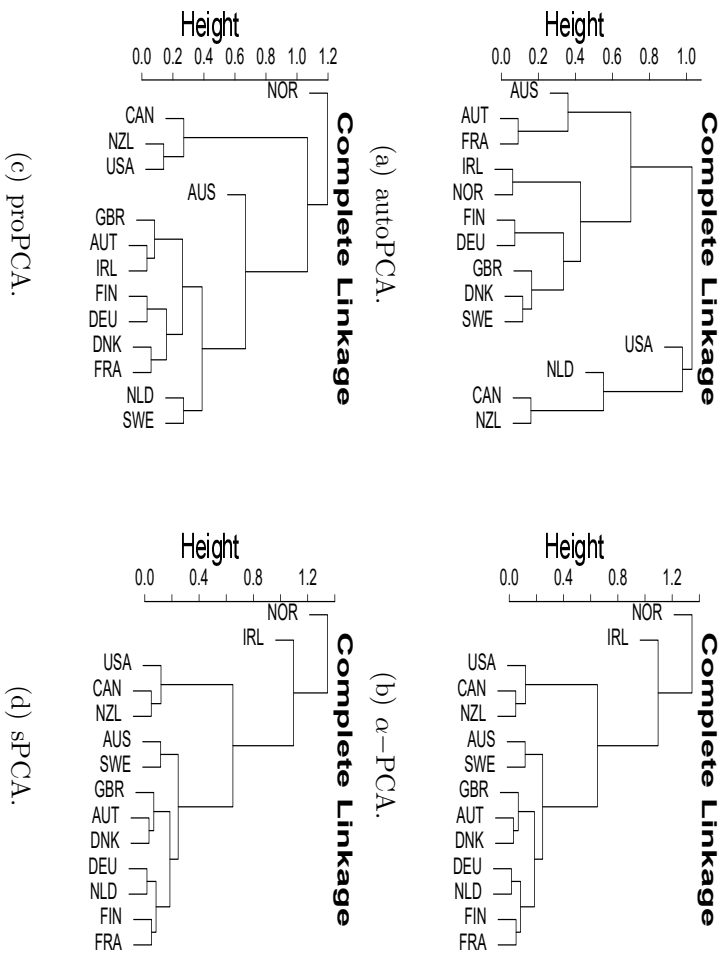


Figure 8: Hierarchical clustering results from the estimated row loading matrix for four different methods of estimation applied to the multinational, macroeconomic indices data.

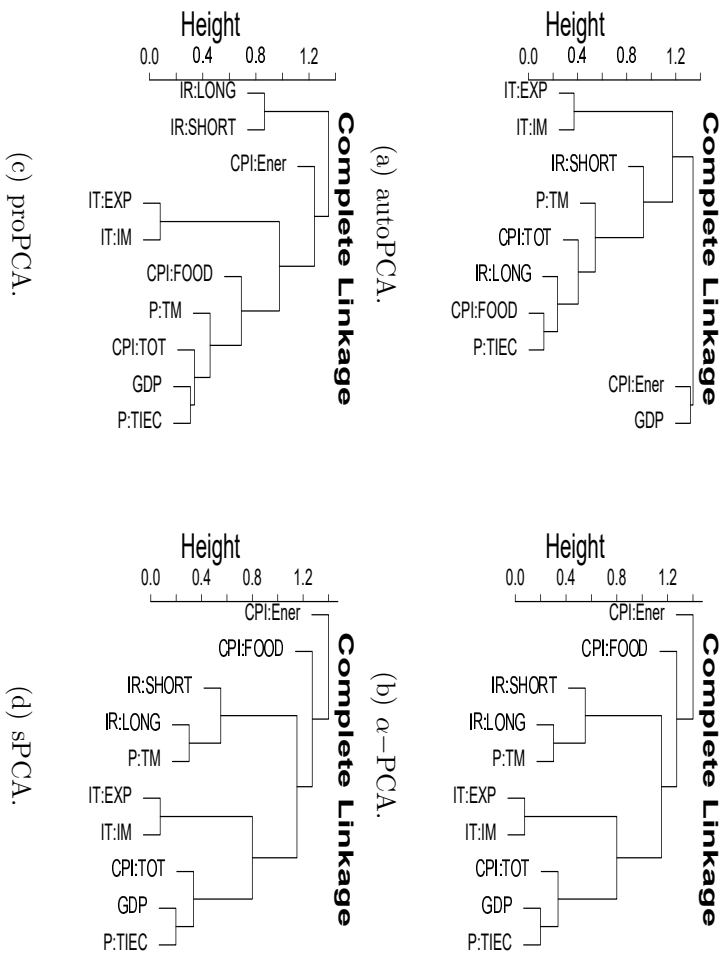


Figure 9: Hierarchical clustering results from the estimated column loading matrix for four different methods of estimation applied to the multinational, macroeconomic indices data.

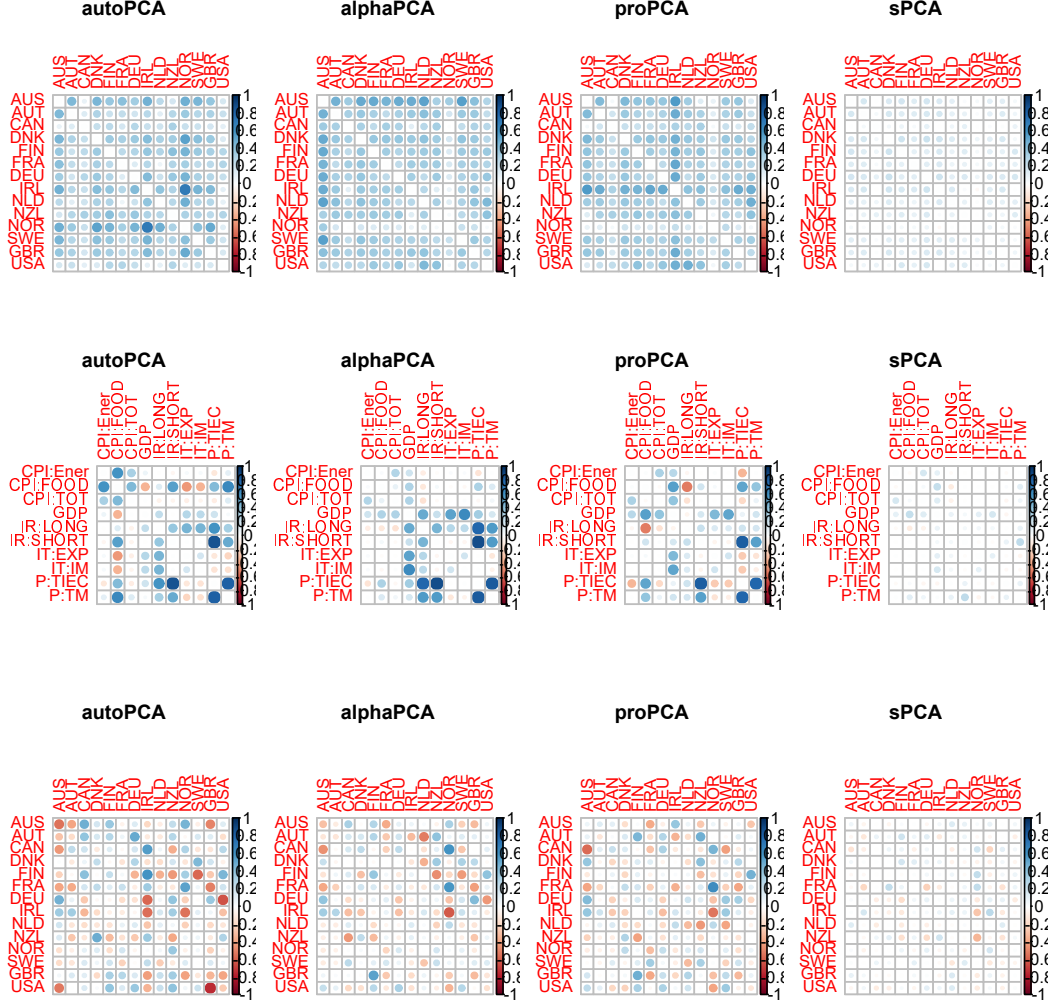


Figure 10: Differences between estimated and observed correlations in the multinational, macroeconomic indices data. The first row gives row-wise results, the second row gives the column-wise results, and the last row gives the interaction between rows and columns result.

Table 3: RMSEs of four estimation methods for different choices of  $(k_1, k_2)$  applied to the multinational, macroeconomic indices data.

Model	Method $/(k_1, k_2)$	(2, 2)	(3, 4)	(5, 6)	(8, 8)
	autoPCA	0.3232	0.2736	0.2272	0.1743
BiMFaM	$\alpha$ -PCA	0.3075	0.2596	0.2142	0.1576
	proPCA	0.3103	0.2608	0.2068	0.1578
RaDFaM	sPCA	<b>0.1979</b>	<b>0.1480</b>	<b>0.0880</b>	<b>0.0429</b>

better than the others.

## 7 Future Research

From the perspective of tensor decompositions, one may rewrite the signal part of BiMFaM and rank- $l$  decomposition part of RaDFaM respectively as follows,

$$\mathbf{R}\mathbf{Z}\mathbf{C}^\top = \mathbf{Z} \times_1 \mathbf{R} \times_2 \mathbf{C} \quad \text{and} \quad \sum_{i=1}^l \mathbf{U}_i \mathbf{V}_i^\top = \sum_{i=1}^l \mathbf{U}_i \circ \mathbf{V}_i.$$

That is, the latent structure of BiMFaM is a special mode-2 case of Tucker decomposition, and the rank- $l$  part of RaDFaM is a special mode-2 case of CANDECOMP/PARAFAC (CP) decomposition (Kolda and Bader, 2009, Sections 3 and 4).

Due to the stronger signal intensity of RaDFaM than BiMFaM, we may conjecture that, once the hierarchical spirit of RaDFaM is extended to tensor-variate observations, the induced new tensor factor model may have stronger signal intensity compared to Tucker tensor factor model raised by Chen et al. (2022), which is actually an extension of BiMFaM under time series setting (Wang et al., 2019). Specifically, for any  $D$ th-order tensor  $\mathcal{X} \in \mathbb{R}^{p_1 \times \cdots \times p_D}$ , we postulate the below hierarchical tensor factor model

$$\begin{cases} \mathcal{X} = \sum_{i=1}^l \mathbf{U}_{1,i} \circ \cdots \circ \mathbf{U}_{D,i}, \\ \mathbf{U}_{d,i} = \mathbf{R}_d \mathbf{A}_{d,i} + \boldsymbol{\xi}_{d,i}, \quad d \in [D]. \end{cases}$$

For this model, it is natural to consider developing estimation procedures that need to build EM-variant algorithm if one seeks the maximum likelihood type estimators.

## SUPPLEMENTARY MATERIAL

**Title:** Supplementary Material for “Factor Modeling of a High-Dimensional Matrix-Variate and Statistical Learning for Matrix-Valued Sequences”

**Overview:** The proof of Proposition 3 is provided in **Appendix A**, the proofs of Theorems 1-4 with the necessary lemmas are provided in **Appendices B-E**, respectively. Additional results for simulations and real data analysis are provided in **Appendices F and G**, respectively.

## References

- Athreya, K. B. and S. N. Lahiri (2006). *Measure Theory and Probability Theory*, Volume 19. Springer.
- Bai, J. (2003). Inferential theory for factor models of large dimensions. *Econometrica* 71(1), 135–171.
- Ben-Israel, A. and T. N. Greville (2003). *Generalized Inverses: Theory and Applications*, Volume 15. Springer Science and Business Media.
- Chang, J., J. He, L. Yang, and Q. Yao (2023). Modelling matrix time series via a tensor cp-decomposition. *Journal of the Royal Statistical Society Series B: Statistical Methodology* 85(1), 127–148.
- Chen, E. Y. and J. Fan (2023). Statistical inference for high-dimensional matrix-variate factor models. *Journal of the American Statistical Association* 118(542), 1038–1055.
- Chen, R., D. Yang, and C.-H. Zhang (2022). Factor models for high-dimensional tensor time series. *Journal of the American Statistical Association* 117(537), 94–116.
- Chen, Z., J. Fan, and D. Wang (2020). High-dimensional factor model and its applications to statistical machine learning. *Scientia Sinica Mathematica* 50(4), 447–490.
- Davis, C. and W. M. Kahan (1970). The rotation of eigenvectors by a perturbation. iii. *SIAM Journal on Numerical Analysis* 7(1), 1–46.
- Dawid, A. P. (1981). Some matrix-variate distribution theory: notational considerations and a bayesian application. *Biometrika* 68(1), 265–274.

- Fan, J., R. Li, C.-H. Zhang, and H. Zou (2020). *Statistical Foundations of Data Science*. Chapman and Hall/CRC.
- Fan, J., Y. Liao, and M. Mincheva (2013). Large covariance estimation by thresholding principal orthogonal complements. *Journal of the Royal Statistical Society Series B: Statistical Methodology* 75(4), 603–680.
- Fan, J., C. Ma, and Y. Zhong (2021). A selective overview of deep learning. *Statistical Science: A Review Journal of the Institute of Mathematical Statistics* 36(2), 264–290.
- Fosdick, B. K. and P. D. Hoff (2014). Separable factor analysis with applications to mortality data. *The Annals of Applied Statistics* 8(1), 120.
- Francq, C. and J.-M. Zakoian (2019). *GARCH Models: Structure, Statistical Inference and Financial Applications*. John Wiley and Sons.
- Greub, W. (1978). Multilinear algebra, universitext.
- Guo, X., X. Liu, E. Zhu, and J. Yin (2017). Deep clustering with convolutional autoencoders. In *International Conference on Neural Information Processing*, pp. 373–382. Springer.
- Gupta, A. K. and D. K. Nagar (2018). *Matrix Variate Distributions*, Volume 104. CRC Press.
- He, X., D. Cai, and P. Niyogi (2005). Tensor subspace analysis. *Advances in Neural Information Processing Systems* 18.
- Hinton, G. E. and R. R. Salakhutdinov (2006). Reducing the dimensionality of data with neural networks. *Science* 313(5786), 504–507.
- Hoff, P. D. (2011). Separable covariance arrays via the Tucker product, with applications to multivariate relational data. *Bayesian Analysis* 6(2), 179–196.
- Kolda, Tamara, G. and W. Bader, Brett (2009). Tensor decompositions and applications. *SIAM Review* 51(3), 455–500.
- Lam, C. and Q. Yao (2011). Estimation of latent factors for high-dimensional time series. *Biometrika* 98(4), 901–918.

- Lam, C. and Q. Yao (2012). Factor modeling for high-dimensional time series: inference for the number of factors. *The Annals of Statistics* 40(2), 694–726.
- Li, B., M. K. Kim, and N. Altman (2010). On dimension folding of matrix-or array-valued statistical objects. *The Annals of Statistics* 38(2), 1094–1121.
- Lu, H., K. N. Plataniotis, and A. Venetsanopoulos (2013). *Multilinear Subspace Learning: Dimensionality Reduction of Multidimensional Data*. CRC Press.
- Salomon, D. (2004). *Data Compression: the Complete Reference*. Springer Science and Business Media.
- Stock, J. H. and M. W. Watson (2002). Forecasting using principal components from a large number of predictors. *Journal of the American Statistical Association* 97(460), 1167–1179.
- Suetens, P. (2017). *Fundamentals of Medical Imaging*. Cambridge University Press.
- Wang, D., X. Liu, and R. Chen (2019). Factor models for matrix-valued high-dimensional time series. *Journal of Econometrics* 208(1), 231–248.
- Yang, X., X. He, J. Zhao, Y. Zhang, S. Zhang, and P. Xie (2020). COVID-CT-dataset: a CT image dataset about COVID-19. *arXiv preprint arXiv:2003.13865*.
- Yu, L., Y. He, X. Kong, and X. Zhang (2022). Projected estimation for large-dimensional matrix factor models. *Journal of Econometrics* 229(1), 201–217.
- Zhang, X. (2017). *Matrix Analysis and Applications*. Cambridge University Press.